


Quantifying the progression of non-alcoholic fatty liver disease in human biomimetic liver microphysiology systems with fluorescent protein biosensors

Manush Saydmohammed^{1,*} , Anupma Jha^{1,*}, Vineet Mahajan^{1,*}, Dillon Gavlock¹, Tong Ying Shun¹, Richard DeBiasio¹, Daniel Lefever¹, Xiang Li¹, Celeste Reese¹, Erin E Kershaw², Vijay Yechoor², Jaideep Behari^{3,4}, Alejandro Soto-Gutierrez^{5,6}, Larry Verneti^{1,7}, Andrew Stern^{1,7}, Albert Gough^{1,7}, Mark T Miedel^{1,7}  and D Lansing Taylor^{1,6,7}

¹University of Pittsburgh Drug Discovery Institute, University of Pittsburgh, Pittsburgh, PA 15261, USA; ²Department of Medicine, Division of Endocrinology and Metabolism, University of Pittsburgh, Pittsburgh, PA 15261, USA; ³Department of Medicine, Division of Gastroenterology, Hepatology and Nutrition, Pittsburgh, PA 15261, USA; ⁴UPMC Liver Clinic, University of Pittsburgh, Pittsburgh, PA 15261, USA; ⁵Department of Pathology, University of Pittsburgh, Pittsburgh, PA 15261, USA; ⁶Pittsburgh Liver Research Center, University of Pittsburgh, Pittsburgh, PA 15261, USA; ⁷Department of Computational and Systems Biology, University of Pittsburgh, Pittsburgh, PA 15261, USA

Corresponding authors: Mark T Miedel. Email: mmiedel@pitt.edu; D Lansing Taylor. Email: dltaylor@pitt.edu

*Co-first authors.

Impact statement

Metabolic syndrome is a complex disease that involves multiple organ systems including the liver. Non-alcoholic fatty liver disease (NAFLD) is a key expression of the metabolic syndrome in the liver. There are no approved therapeutics to halt or reverse the progression of NAFLD. Human biomimetic liver MPS, harnessing fluorescent protein biosensors (FPBs) to quantify the temporal-spatial changes in pathophysiological parameters during disease progression, have the potential to serve as an important component of an experimental platform for both drug repurposing and novel therapeutic development. FPBs can be applied as biomarkers in key pathways, and to molecular targets identified from patient genomic data, to monitor disease progression and responses to drug treatment. The integration of QSP, human biomimetic MPS with FPBs, and the MPS database described here offers a powerful platform for identifying mechanisms and biomarkers of metabolic disease progression, as well as identifying new therapeutic strategies.

Abstract

Metabolic syndrome is a complex disease that involves multiple organ systems including a critical role for the liver. Non-alcoholic fatty liver disease (NAFLD) is a key component of the metabolic syndrome and fatty liver is linked to a range of metabolic dysfunctions that occur in approximately 25% of the population. A panel of experts recently agreed that the acronym, NAFLD, did not properly characterize this heterogeneous disease given the associated metabolic abnormalities such as type 2 diabetes mellitus (T2D), obesity, and hypertension. Therefore, metabolic dysfunction-associated fatty liver disease (MAFLD) has been proposed as the new term to cover the heterogeneity identified in the NAFLD patient population. Although many rodent models of NAFLD/NASH have been developed, they do not recapitulate the full disease spectrum in patients. Therefore, a platform has evolved initially focused on human biomimetic liver microphysiology systems that integrates fluorescent protein biosensors along with other key metrics, the microphysiology systems database, and quantitative systems pharmacology. Quantitative systems pharmacology is being applied to investigate the mechanisms of NAFLD/MAFLD progression to select molecular targets for fluorescent protein biosensors, to integrate computational and experimental methods to predict drugs for repurposing, and to facilitate novel drug development. Fluorescent protein biosensors are critical components of the platform since they enable monitoring of the pathophysiology of disease progression by defining and quantifying the temporal and spatial dynamics of protein functions in the biosensor cells, and serve as

minimally invasive biomarkers of the physiological state of the microphysiology system experimental disease models. Here, we summarize the progress in developing human microphysiology system disease models of NAFLD/MAFLD from several laboratories, developing fluorescent protein biosensors to monitor and to measure NAFLD/MAFLD disease progression and implementation of quantitative systems pharmacology with the goal of repurposing drugs and guiding the creation of novel therapeutics.

Keywords: Fluorescent protein biosensors, metabolic syndrome, non-alcoholic fatty liver disease, metabolic dysfunction-associated fatty liver disease, type 2 diabetes, microphysiology systems, quantitative systems pharmacology

Experimental Biology and Medicine 2021; 246: 2420–2441. DOI: 10.1177/15353702211009228

Introduction

This perspective describes the state of the integration of QSP,¹ human biomimetic liver MPS,^{2,3} FPBs,^{4,5} and the microphysiology systems database (MPS-Db)^{6,7} to create a platform for investigating the temporal-spatial mechanisms of metabolic syndrome disease progression, starting with the liver. A part of QSP, the iterative computational and experimental approach to drug discovery and development, has been harnessed to characterize NAFLD and type 2 diabetes (T2D) in patient liver samples by RNASeq.⁸ Computational and systems biology tools have then been applied to the patient RNASeq data to predict pathways, networks, and molecular targets involved in the progression of NAFLD/T2D in an unbiased approach.^{9–14} This knowledge has been used to computationally predict drugs/compounds for repurposing and as a starting point for designing novel therapeutics using human biomimetic liver MPS disease models.^{15–18} FPBs are a critical component of the platform since they can be used to define the temporal-spatial changes that characterize the progression of the disease, serve as biomarkers of disease progression, as well as response to prospective therapeutic treatments in the human biomimetic liver MPS. The evolution of this platform will be compared to previous studies harnessing human biomimetic MPS experimental models of NAFLD/NASH.

Metabolic syndrome, NAFLD, and metabolic dysfunction-associated fatty liver disease

Metabolic syndrome is a complex disease that exhibits temporal-spatial dynamics within individual organs, such as the spatial variation of metabolic functions within the zoned liver acinus.¹⁹ Abdominal adipose tissue, pancreatic islets, muscle (striated and cardiac), liver, and portal endothelium are key tissues involved in metabolic syndrome²⁰ (Figure 1). In a healthy pancreas, insulin production and release are regulated by blood glucose. Blood glucose levels are also influenced by hepatic glucose production and peripheral glucose uptake (e.g. by muscle and adipose tissue). With a sedentary lifestyle and an unhealthy diet containing high glucose and fatty food, excess fat accumulates in the adipose tissue as well as “ectopically” in non-adipose tissues, thereby promoting insulin resistance. During the progression of metabolic syndrome from a prediabetic to a diabetic state, there is an excessive demand for insulin to overcome the insulin resistance. The failure to meet this insulin demand results in pancreatic β cell dysfunction and loss that leads to impaired insulin secretion, hypoinsulinemia, and hyperglycemia. This relative insulin deficiency reduces insulin’s suppressive effects on adipose tissue lipases, adipose triglyceride lipase (ATGL), and hormone sensitive lipase (HSL), which lead to increase lipolytic release of free fatty acids (FFAs). This sequence of events

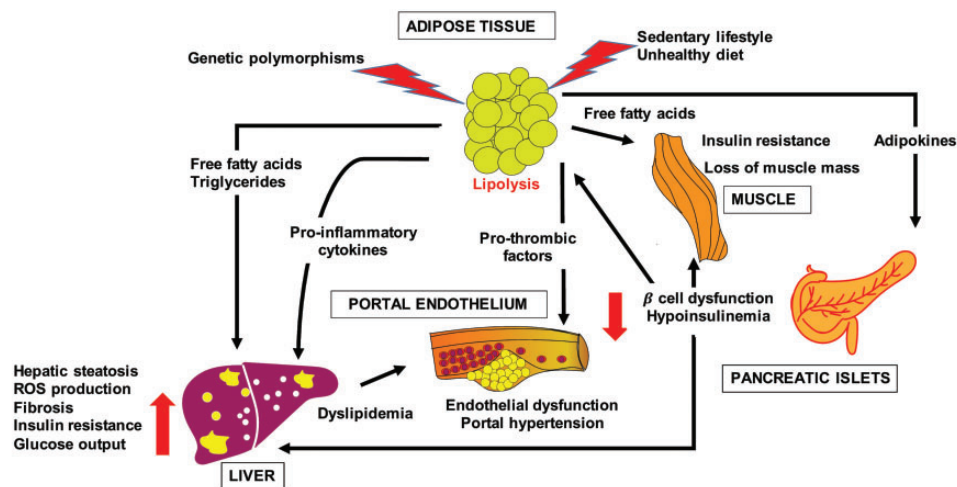


Figure 1. An overview of the mechanisms involved in the progression of metabolic syndrome. In a healthy pancreas, insulin production and release are regulated by blood glucose levels that reflect glucose uptake in muscle and adipose tissue along with uptake and secretion from the liver. As a result of poor diet, sedentary lifestyle, and/or genetic polymorphisms there is excessive demand for insulin to metabolize glucose. The failure to meet this insulin demand results in pancreatic β cell loss and impaired insulin production, driving the progression of metabolic syndrome from prediabetes to diabetes state. Low insulin levels in adipose tissue promotes lipolysis of fat and release of FFAs, triglycerides as well as proinflammatory cytokines and adipokines, that are delivered to the liver through circulation, promoting hepatic steatosis, reactive oxygen species (ROS) production, fibrosis, increase in glucose output, and insulin resistance. Further, hepatic lipolysis of triglycerides leads to dyslipidemia, endothelial dysfunction, portal hypertension along with proinflammatory and prothrombotic factors in the circulation that contribute to cardiovascular disease and stroke (Figure adapted from literature^{21–26}).

further increases ectopic lipid storage and insulin resistance in peripheral tissues as well as increased hepatic secretion of triglyceride-rich lipoproteins. The latter leads to high serum triglycerides and low HDL-cholesterol, which is characteristic of the metabolic syndrome. In addition, proinflammatory cytokines released from adipose tissue and delivered to the liver through the vasculature promote inflammation. Together, these processes further increase *de novo* lipogenesis, gluconeogenesis, steatosis, inflammation, reactive oxygen species (ROS), and fibrosis in the liver. Ultimately, these changes lead to additional deleterious manifestations of the metabolic syndrome including endothelial dysfunction, and portal hypertension, along with an increase in proinflammatory and prothrombotic factors in circulation that also contribute to cardiovascular disease and stroke.

It is estimated that up to 70% of T2D patients have coexisting NAFLD.^{20–22,27–29} It has been suggested that NAFLD represents a key liver manifestation of the metabolic syndrome in patients.²² Liver insulin resistance is also a common feature in NAFLD patients, furthering the link between NAFLD and T2D/metabolic syndrome. NAFLD consists of a spectrum of disease stages ranging from simple steatosis, to nonalcoholic steatohepatitis (NASH) that includes hepatocyte ballooning, inflammation, and pericellular fibrosis.^{30,31} In some patients, NASH progresses to cirrhosis, liver failure, and hepatocellular carcinoma (HCC).^{22,32} Currently, NASH is the most rapidly growing indication for liver transplantation.^{33,34}

Fatty liver linked to a range of metabolic dysfunctions occurs in approximately 25% of the population. Recently, a panel of experts agreed that the acronym, NAFLD, did not properly characterize this heterogeneous disease that can include metabolic dysfunctions such as T2D, obesity, and hypertension that are components of the metabolic syndrome.³⁵ Therefore, metabolic dysfunction-associated fatty liver disease (MAFLD) has been proposed as the new term to cover the heterogeneity identified in the NAFLD patient population. Unfortunately, there are still no approved drugs to halt or reverse the progression of NAFLD,³⁶ now MAFLD³¹. The complexity and heterogeneity of NAFLD/MAFLD in patients, variability in the rate of disease progression to advanced fibrosis/cirrhosis over several decades in some patients and rapid progression in other patients (ca. 20%), along with the coupled comorbidity with T2D, probably account for the present failure to develop effective therapies.²² In addition, it is now understood that convergent factors beyond the range of comorbidities, including genetic risk factors, environment, microbiome and metabolism, play important roles in the disease heterogeneity.³²

Chronic progression of fatty liver disease in the liver has been demonstrated in animal models and some *in vitro* experimental disease models by a variety of measured characteristics including increased steatosis, oxidative stress, ER stress, apoptosis, autophagy, insulin resistance, and fibrogenesis^{3, 23, 37–41} (Figure 1). Despite years of efforts studying the progression of human NAFLD in animals, an optimal *in vivo* model suitable for all types of studies does not exist. For example, the traditional genetic mouse

models of NAFLD (leptin deficient *ob/ob* or leptin receptor deficient *db/db* mouse models) will progress to liver steatosis but not to NASH without additional challenges from LPS or specialized diets.^{42,43} The nutrient deficient models, such as the methionine and choline deficient diet in the mouse, will lead to hepatic steatosis, liver inflammation, injury, and fibrosis but also induce weight loss and increase insulin sensitivity resulting in lower glucose, both of which are metabolic changes contrary to the clinical progression in NAFLD/MAFLD.⁴⁴ High-fat diet rodent models of liver diseases lead to obesity, insulin resistance, liver inflammation, and fibrosis but suffer from high variability between animals and require treatments for one year or longer.⁴⁵ However, the addition of high fructose to a high fat diet has been found to shorten the treatment time required to mimic human NASH with fibrosis to four to six months.⁴⁶ In recent years, studies of the effects of metabolic syndrome on the liver are increasingly incorporating metabolic and transcriptomic analyses to correlate changes in the profiles with histopathology changes in human disease.³² However, animal models that mimic the histopathology of human liver diseases often do not exhibit the changes in genes, pathways, and networks associated with human disease progression, suggesting the molecular mechanisms are different from humans,³² emphasizing the need for patient-derived MPS (see below).

In addition, genetic factors have been identified that contribute to NAFLD development and progression.^{47,48} Most of these genetic variants are related to regulation of lipid biology including PNPLA3, MBOAT7, TM6SF2, and GCKR⁴⁴. It is well known that subsets of the overall population of patients with NAFLD/MAFLD carry specific gene variants that enhance or reduce disease risk, as demonstrated by association studies.⁴⁹ For instance, the PNPLA3 I148M variant carriers evaluated by non-invasive imaging and gene expression methods showed lower *de novo* lipogenesis and a higher content of polyunsaturated fatty acids than non-carriers.⁵⁰ Most of these genetic variants are difficult to study in animal models of NAFLD/MAFLD.

Computational analyses of differences in genomic data (e.g. RNASeq) between normal and diseased patient liver biopsies reveal changes in gene signatures within pathways that are either up or down regulated as part of the disease progression^{8,9,12,14,16–18} (Figure S1). Molecular targets within the most significant pathways (a few examples are shown in Figure S1) could be harnessed by constructing fluorescent protein biosensors (FPBs) that would be used to monitor the disease progression over time and space using human MPS. Selected pathways shown here, which were determined by identifying key biomarkers in the disease spectrum from early NAFLD to T2D in liver patients, are some of the key candidates selected to guide the development of FPBs for the expression of metabolic syndrome in the liver.⁵¹ Developing FPBs is a vital step in quantifying the progression of NAFLD/MAFLD and identifying potential biomarkers in organ MPS, starting with the liver. MAFLD will be used as the general term to express the heterogeneity in these patient populations, although NAFLD will be used when referring to published studies before the new language was proposed.

Human MPS to investigate metabolic syndrome

Human MPS, also referred to as tissue chips and organ-on-chips, are 3D microfluidic devices containing multiple cell types to enable cell-to-cell communications and additional physical and biochemical cues that recapitulate some structural and functional characteristics of organs.^{2,3,52} There are multiple types of MPS including high throughput⁵³ and high content versions that meet the “fit for purpose” or “context of use” requirements in the drug discovery/development pipeline.² We have focused on high content human MPS that maximally recapitulate the organ structure and functions. We refer to this type of MPS as a “human biomimetic MPS”.³ We have continuously evolved and improved the human biomimetic liver MPS models to address the complexity of studying absorption, distribution, metabolism, excretion and toxicity (ADMET),^{19,51,54} as well as disease models including MAFLD/metabolic syndrome^{38,39,51} and liver metastases,^{55,56} using different versions of the models including: the sequentially layered, self-assembly liver (SQL-SAL);⁵¹ the liver acinus MPS (LAMPS);³⁸ and the vascularized liver acinus MPS (vLAMPS).³⁹ A variety of other human liver MPS have been harnessed in the study of NAFLD/MAFLD.^{3,37,40} We have recently reviewed the development and challenges in designing, constructing, and applying human biomimetic MPS.³

Presently, we apply both the LAMPS³⁸ and vLAMPS³⁹ models for toxicology and disease modeling, as well as drug discovery. These models contain primary human hepatocytes, primary human liver sinusoidal endothelial cells (LSECs), together with well-characterized human stellate and Kupffer cell lines. The LAMPS is a simpler model with a single channel in which the cells are layered sequentially to recreate the 3D organization of the liver sinusoid.

The LAMPS can be run with either zone 1 or zone 3 oxygen tension conditions to explore zone-specific physiology and pathophysiology, and can be imaged in real-time to monitor FPBs. The LAMPS has been tested and reproduced by the Texas A&M Tissue Chip Validation Center (Tex-Val) one of the National Center for Advancing Translational Sciences (NCATS) funded Tissue Chip Testing Centers (TCTC).⁵⁷ Results of that testing can also be found in the MPS-Database.^{6,7,58} The vLAMPS (Figure 2(a)) uses a two channel glass device to create an upper hepatic channel and a lower vascular channel, separated by a 3- μ m pore size PET membrane (shown as a red dotted line). The vLAMPS generates an oxygen gradient through the consumption of oxygen by the hepatocytes, recapitulating physiological zonation in the liver.³⁹ The application of the vLAMPS is evolving toward the use of all patient-specific primary cells, including immune cells for the optimal modeling of disease progression, in advance of the ability to employ fully matured induced pluripotent stem cell (iPSC)-derived cells.³ Patient-specific, iPSC-derived parenchymal, and non-parenchymal cells, including cholangiocytes, are currently being developed for the next generation vLAMPS^{3,60–62} and more macro mini livers that also mimic many aspects of NAFLD/MAFLD.⁶³ Success with the maturation of all liver acinus cells from patient-derived iPSCs will create a platform for preclinical trials and personalized medicine.³ The vLAMPS can be run as a stand-alone human biomimetic liver MPS or be coupled through the vascular channel to other disease relevant organ MPS (Figure 2(b)). Table S1 compares the advantages and disadvantages of using LAMPS and vLAMPS. Independent testing of the vLAMPS by the Tex-Val TCTC has been initiated.

A standalone liver MPS can be harnessed to study the progression of metabolic syndrome by modifying the

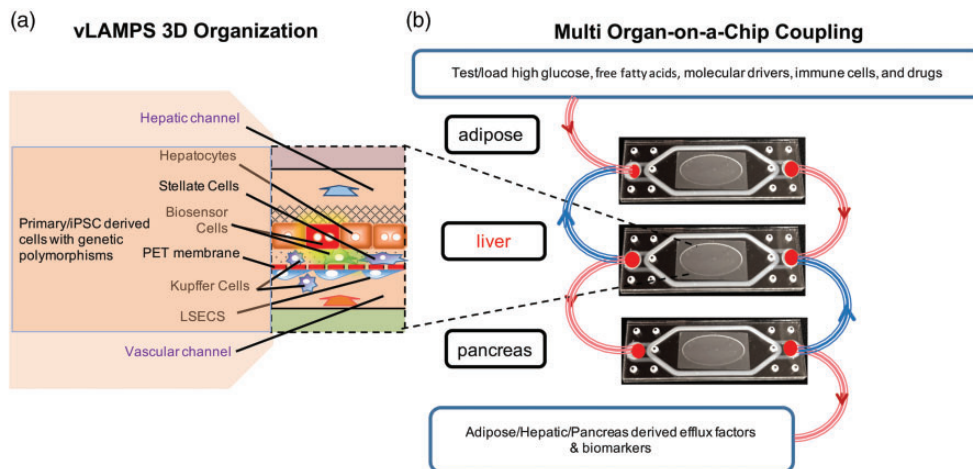


Figure 2. Evolving multi-organ, biomimetic MPS models for investigating metabolic syndrome. The evolution of liver MPS models to understand metabolic syndrome was described previously.^{3,38,51} (a) The vascular liver acinus MPS (vLAMPS) contains the upper hepatic channel and lower vascular channel separated by a PET membrane (red dashed line). The vLAMPS presently uses primary human cells (hepatocytes and Liver Sinusoidal Endothelial Cells, LSECs), immortalized human cell lines for stellate (LX-2) and Kupffer (activated THP-1 cells). To mimic the progression of metabolic syndrome in vLAMPS, molecular drivers (e.g. high glucose, cytokines, free fatty acids, and lipopolysaccharide) and inflammatory immune cells are selectively added to vascular channels. (b) Selected organ MPS models relevant to metabolic syndrome can be functionally coupled by transferring efflux from other organ MPS,⁵⁴ or by direct coupling of the vLAMPS, adipose MPS, and pancreatic (vPANIS) through the vascular channels,⁵⁹ both of which allow the addition of molecular drivers, immune cells, and potential therapeutics. The direction of media flow is indicated by red/blue color-coded lines and arrows. For MPS models, the development and use of fluorescent protein biosensor (FPB) cells are critical for real-time and spatial monitoring of the progression of metabolic syndrome.

media from normal fasting through early metabolic syndrome (MAFLD) to late metabolic syndrome (T2D) (Table 2). Selected organ MPS models relevant to metabolic syndrome can also be linked by functional coupling (transfer of efflux from one organ MPS as influent to another organ MPS)^{54,59} or by physical coupling, such as coupling an adipose MPS (AMPS) and/or pancreatic islets MPS (vPANIS) to the vLAMPS (Figure 2(b)). The direct fluidic coupling of the vLAMPS, AMPS, and vPANIS through the vascular channels allows the addition of molecular drivers of disease, immune cells, and potential therapeutics. In Figure 2(b), the direction of media flow from each organ is indicated by red/blue color-coded lines and arrows. The forward loop (red lines) indicates the sequential flow of vascular media from the AMPS, to the vLAMPS, to the vPANIS, to evaluate the effect of effluent factors on the downstream organ models. The feed-back loops (blue lines) indicate the option to recirculate media between coupled organs to test the combined effects of efflux components on pairs of organs, to determine how vascular factors contribute to the progression of metabolic syndrome. Organ-derived efflux factors and biomarkers serve as secreted metrics by which disease progression can be evaluated. However, the concurrent use of FPBs in hepatocytes and non-parenchymal cells is essential for real-time and spatial monitoring (e.g. zone-specific measurements in the vLAMPS) of the progression of metabolic syndrome. Therefore, developing FPBs and additional efflux biomarkers is critical for monitoring the progression and understanding the mechanisms of metabolic syndrome and its response to therapeutics.

Fluorescent protein biosensors

The history of FPBs dates back to early methods to track the dynamics of fluorescently labeled, purified proteins put back into living cells, called fluorescent analogs.⁷⁰ The concept of modifying proteins with environmentally sensitive fluorescent probes at sites known to be involved in ligand binding led to the development of a variety of FPBs using purified proteins,^{5,71} even before the development of fluorescent protein- (e.g. GFP) engineered FPBs.^{72,73} Over the last 20 years, many specific fluorescent protein-based FPBs have been designed, developed, and applied to many types of cells in 2D and 3D.^{4,74,75} To avoid potential artifacts from engineered cells, as a rule, only ca. 10–20% of the cells of any cell type in an MPS are induced to express FPBs.⁴ This allows the temporal-spatial monitoring of specific FPBs in any cell type in the MPS, while maintaining most of the cells as native. Multiple FPBs can be analyzed in a single MPS by spectral selection of the fluorescent proteins used to construct the FPBs.⁴

Key features of FPBs include: the reversibility, sensitivity, and dynamic range of biosensor response, the ability to define and quantify temporal and spatial dynamics of protein functions in the cells, and the ability to serve as a minimally invasive biomarker of a physiological state of the organs or cells.⁴ There are three major types of FPBs⁴ (Figure 3). In one type of FPB, conformation-sensitive biosensors, ligand binding (e.g. metabolites, proteins and peptides) to the sensing domain of the FPB, or cleaving of a

specific sequence in the FPB, modulate the fluorescence intensity and/or lifetime, providing a real-time readout of the physiological process being monitored (Figure 3(a)). In a second type of FPB, localization biosensors, activation of a specific pathway in the cell result in the post-translational modification of the FPB, exposing a nuclear import/export sequence that guides the translocation of the FPB (Figure 3 (b)). In a third type of FPB, activation-dependent biosensors, an FPB fusion protein driven by a gene specific promoter increase the reporter expression on activation, generating a fluorescent readout (Figure 3(c)). Examples of FPBs that are especially relevant to MAFLD, and can be incorporated into organ MPS and/or organoids, are shown in Table 1. Presently, we have focused on the use of lentiviral delivery of the FPBs to targeted cells since cell lines, primary cells, and iPSC-derived cells can all be readily transduced by lentivirus. However, other methods for delivery are possible, including the use of clustered regularly interspaced short palindromic repeats (CRISPR).⁴

Examples of the design and working principles of a conformation sensitive ROS-FPB and a localization-based insulin resistance-FPB are illustrated in Figure S2. Generation of ROS resulting from nutrient overload and mitochondrial dysfunction contributes to the development of hepatic insulin resistance. To develop an ROS-FPB (Figure S2(a)), a conformation sensitive fluorescent protein, CP-YFP, is cloned with a linker domain between the oxidation sensitive bacterial transcription factor Oxy-R-domains. In the presence of ROS (e.g. an increase in H₂O₂), the reduced thiol form (-SH) within cysteine is oxidized and forms a disulfide (S-S) bond, altering the conformation of the fluorescent protein and increasing the fluorescence intensity of the CP-YFP.⁷⁷ In the context of the second example, insulin resistance can be detected as activation of the Forkhead transcription factor (FOXO1), a critical transcriptional activator in the insulin signaling pathway,¹⁰³ with a localization FPB. In healthy hepatocytes, during the fed/high insulin state, FOXO1 expression is limited to the cytoplasm. However, in the fasted/low insulin state, FOXO1 translocates to the nucleus where it mediates adaptive transcriptional responses (e.g. regulation of genes involved in gluconeogenesis and glycogenolysis). However, in insulin-resistant hepatocytes, the nuclear-cytoplasmic shuttling mechanism is impaired and FOXO1 remains in the nucleus.¹⁰⁴ To create an insulin resistance FPB (IR-FPB), FOXO1 was engineered with a fluorescent protein tag to indicate insulin resistance.¹⁰⁵ Specifically, as insulin resistance increases, so does the insulin-independent localization of the IR-FPB in the nucleus, and the percentage of cells with the IR-FPB localized in the nuclei (Figure S2(b)). To prevent the IR-FPB from interfering with (i.e. modulating) the metabolic signaling pathway, a mutation is created in the FOXO1 DNA binding domain (H215R) that limits its transcriptional activity.

The steps involved in developing, testing, and implementing FPBs, using the ROS-FPB and the IR-FPB as examples, are outlined in Figure 4(a). FPBs are first transiently transfected in cell lines to confirm expression and function. Improving the efficiency of integration is accomplished by lentiviral packaging of the FPB and transduction into the

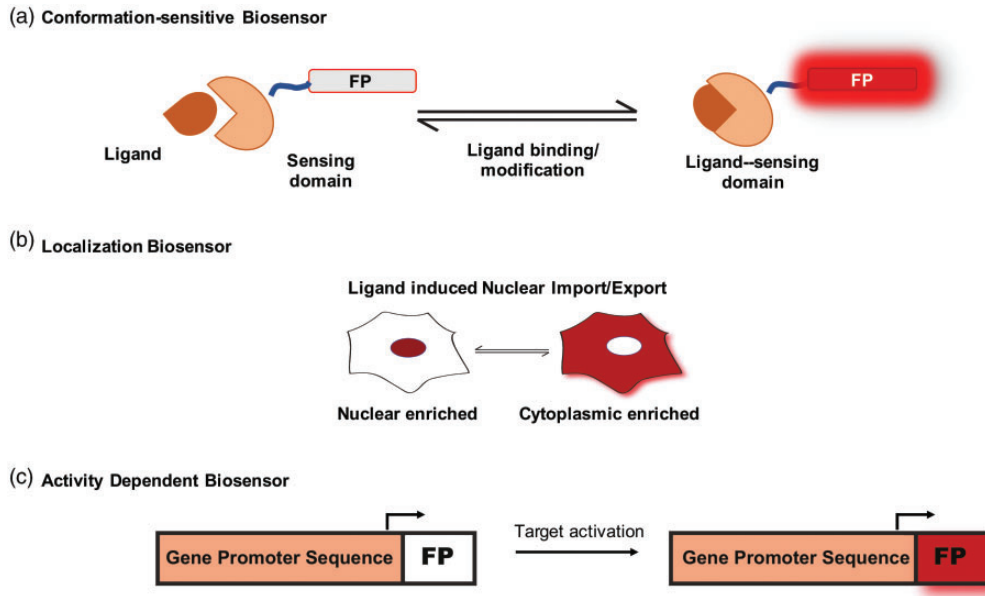


Figure 3. Types of fluorescent protein biosensors. (a) Conformation sensitive biosensor: A protein conformation change upon ligand binding activates/modifies the fluorescent signal intensity and/or color, which provides a readout of changes in ligand concentration. (b) Localization biosensor: Activation of a specific pathway results in post-translational modification of the protein to expose a target localization sequence in the biosensor guiding translocation to the target cellular location after. (c) Activity-dependent biosensor: This is a fusion protein driven by a specific gene promoter where upon activation of the promoter increases the reporter expression, which provides a fluorescent readout.^{4,76}

selected cells to test for consistent biosensor expression and function. FPBs are then transduced into primary hepatocytes and/or non-parenchymal cells prior to incorporation into LAMPS or vLAMPS. Additionally, CRISPR-mediated targeted integration is being used to create FPB expressing iPSCs (work in progress). To test the ROS-FPB, human hepatocytes were transduced and incubated with either NF, EMS, or LMS media for seven days. Increased fluorescence of the ROS biosensor was observed in EMS and LMS media relative to NF media (Table 2, Figure 4(b)). Measurement of the mean total fluorescence intensity per field demonstrated a significant increase in ROS biosensor activity in response to EMS and LMS media that is consistent with the progression of MAFLD (Figure 4(c)). Initial testing of the IR-FPB used HepG2 cells, which are easily transfected with GFP-FOXO1, treated with either 50 μ M forskolin or DMSO for 6h, then fixed and labeled with Hoechst for imaging the IR-FPB (Hoechst labeling serves as marker of hepatocyte nuclei, Figure 4(d)). Forskolin, an activator of cyclic AMP signaling, mimics the insulin resistance condition in hepatocytes.^{106,107} Representative images of control and forskolin treated cells show that the expression of FOXO1 is mainly cytosolic in untreated cells (left panel), while nuclear translocation of FOXO1 is observed in forskolin-treated cells (right panel; arrowheads). Quantitation of the percentages of FOXO1-positive nuclei in both control and forskolin-treated cells using the WEKA image classifier (ImageJ) indicated there was a significant increase in the percentage of FOXO1-positive nuclei in forskolin-treated cells (Figure 4(e)). These data demonstrate that the FOXO1 biosensor will be useful for assessing insulin resistance conditions in LAMPS and vLAMPS models under media conditions that support the progression of metabolic syndrome.

The FPBs used to define the temporal-spatial changes within a zoned human biomimetic liver MPS in each study are complemented by the use of in-line sensors for continuous recording of the average value of oxygen tension, glucose, etc.^{108,109} Although FPBs will ultimately be included in all of the organ MPS used to investigate metabolic syndrome, our initial focus is on MAFLD in the liver. We have focused on FPBs as defined above in this perspective. However, there are many other fluorescence-based reagents that can be used in combination with FPBs within MPS to measure cellular functions, as well as photo-activatable proteins that can be used to manipulate cellular functions.

Optogenetics, the use of light to activate proteins, allows dynamic control of the location, timing, and intensity of activation.¹¹⁰ Optogenetics has been successfully used to study biological functions such as neuronal activity, gene regulation, and signaling protein activities. Early research using optogenetics was based on light-responsive ion channels in the Opsin family.¹¹⁰ These optogenetic tools rely on conformational changes in response to the exposure of a specific wavelength of light and dimerization of the light-sensitive protein domain. The number of light-sensitive proteins harnessed as optogenetic tools has increased and include Cryptochrome2 (Cry2/Cry2PHR),¹¹¹ Phytochrome B (PhyB),¹¹² ultraviolet B receptor (UVR8),¹¹³ flavin adenine dinucleotide (BLUF) and light-oxygen-voltage (LOV).¹¹⁴

Recently, optogenetics has been used to study hierarchical signaling in multicellular models including a stem culture of genetically modified human embryonic co-culture cells (hESC). Here the optogenetic stimulation within a subpopulation of cells encoding an optogenetic-protein target was used to study the Wnt signaling pathway.¹¹⁵ Subsequently, optogenetic stimulation and light activation at variable

Table 1. Selected list of genetically encoded FPBs to study the progression of metabolic syndrome.

Fluorescent protein biosensor (FPB)	Sensing domain	Response	Organs or cell lines used	Biological process	References
Nuclear label	Histone 2B (H2B)	Nuclear fluorescence	Liver LX2 cells Kupffer cells	Cell proliferation and translocation	4
Reactive oxygen species	<i>E. coli</i> protein OxyR (OxyR-RD)	Increase in fluorescence	Hepatocyte and beta cells	Oxidative stress reactive oxygen species H ₂ O ₂	27, 77
Insulin Resistance	FoxO1 protein	Nuclear/cytoplasm (translocation)	Hepatocyte, β- cells and adipose tissue	Nuclear import and export	78-86
Lipid accumulation	Perilipin	Increase in fluorescence of lipid droplets	AML12 mouse liver, McARH7777 rat hepatoma cells	Regulation of lipolysis	87-89
ER stress	XBP1, ATF4	Increase in fluorescence	HeLa cell, HCT116 and HEK293T	XBP1 splicing, ATF4 translocation	86, 90-93
Apoptosis	Cytochrome C oxidase VIII subunit	Decrease in fluorescence	Hepatocyte	Cell death	4, 51
Fibrosis	Collagen1A1/A2 promoter	Increase in fluorescent intensity and shift in fluorescence emission	NIH3T3 cells	Collagen production	94, 95
NADH/NAD ⁺ redox coupling	Bacterial NADH binding protein REX	Increase in green-to-red fluorescence ratio	Mouse neuroblastoma	NADH:NAD ⁺ ratio	96, 97
Citrate (tri carboxylic acid cycle) cAMP signaling	CitA from <i>Klebsiella pneumoniae</i> cAMP binding domain of Epac1	Increase in fluorescence Increase in fluorescence	INS-1 cells HeLa cells, Cerebral cortical astrocytes	Citrate levels Cyclic AMP levels	98, 99 100
Hypoxia and cell cycle	Hypoxia responsive element promoter and Geminin	Increase in fluorescence	HEK293T cells in tumor xenograft	S-G2M phase cell cycle and VEGFA promoter activity	101
JNK pathway	C-Jun N-terminal kinase	Nuclear/ Cytosolic (translocation)	NIH3T3, RAW264.7 and HeLa Cells	Nuclear import and export	102

Table 2. Key differences between normal fasting (NF), early metabolic syndrome (EMS) MEDIA, and late metabolic syndrome (LMS) media.

Component	NF (normal fasting)	EMS (early metabolic syndrome; MAFLD)	LMS (late metabolic syndrome; T2D)
Glucose	5.5 mM	11.5 mM	20 mM
Insulin	10 pM	10 nM	10 nM
Glucagon	100 pM	10 pM	10 pM
Oleic acid	–	200 μ M	200 μ M
Palmitic acid	–	100 μ M	100 μ M
LPS	–	–	1 μ g/mL
TGF- β	–	–	10 ng/mL
Glutamine (glutaMAX)	2 mM	2 mM	2 mM

Note: Media formulations were designed to mimic disease progression from normal fasting (NF) to early metabolic syndrome (EMS; MAFLD) and late metabolic syndrome (LMS; T2D). These medias were developed with glucose-free Williams E media supplemented with physiologically relevant levels of glucose, insulin, glucagon, oleic acid, palmitic acid, and molecular drivers of disease including TGF- β and LPS. We then adjusted these components to reflect the pathophysiological conditions.^{64–69}

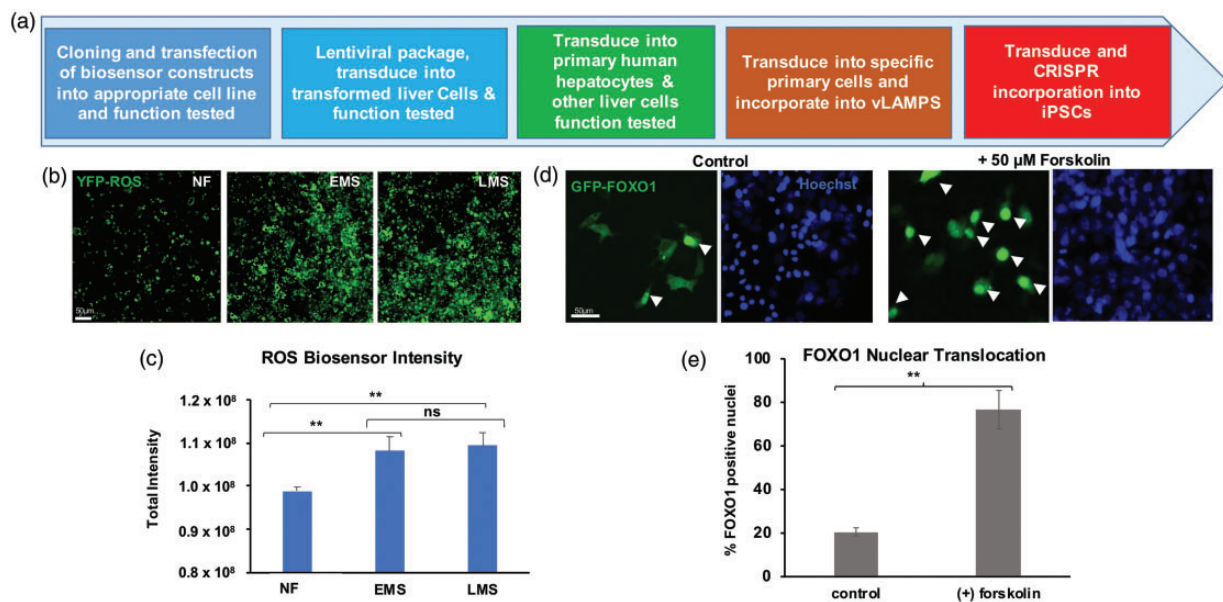


Figure 4. Steps involved in developing, testing, and implementing FPBs. (a) Description of the procedure used for testing FPBs during development. (b) Representative images of primary human hepatocytes that were transduced with a lentiviral packaged ROS biosensor and plated in a collagen coated 96-well plate. Images were acquired with a 20 \times (0.45 NA) objective; Scale bar; 50 μ m. Increased fluorescence of the ROS biosensor is observed after seven days in either EMS or LMS media relative to NF media. (c) Quantitation of the total fluorescence intensity per field in all the images illustrated in part (b) shows a consistent increase in ROS biosensor activity going from NF to EMS to LMS, consistent with progression to MAFLD. (Statistical significance was assessed using a one-way ANOVA with multiple comparisons (Tukey Test): ** $P < 0.01$). (d) Development and testing of an insulin resistance FPB. HepG2 cells were plated in a collagen coated 96-well plate and were transfected with GFP-FOXO1 plasmid, treated with either DMSO or 50 μ M forskolin in DMSO for 6 h, then fixed and labeled with Hoechst before imaging. Representative images show that FOXO1 is predominantly expressed in the cytosol in untreated cells (control), while nuclear translocation of FOXO1 is observed in forskolin-treated cells (+50 μ M Forskolin); arrowheads. Images were acquired with a 20 \times (0.45 NA) objective; Scale bar; 50 μ m. (e) FOXO1-positive nuclei were quantified as percent of total cell count, demonstrating an increase in the percentage of FOXO1-positive nuclei in forskolin-treated cells (unpaired, two-tailed t -test with the assumption of equal variance was used to compare control and forskolin-treated groups; ** $P < 0.01$).

amplitude (LAVA) were used to study dose-dependent Wnt activation.¹¹⁵ The use of the LAVA platform has been suggested to validate multiple signaling pathways in development and cell biology.¹¹⁶ Optogenetics can be used in combination with FPBs to manipulate and measure protein activities in MPS models.

Photoactivable proteins (PA-FPs) exhibit a change in spectral properties after exposure to a specific wavelength of light.¹¹⁷ They can “turn on” labeled proteins in a defined pattern by light activating the fluorescence in order to track a subset of the proteins, or by changing the fluorescence emission to differentiate the spatially activated proteins.

They are categorized as an irreversible PA-FP, a photoconvertible PA-FP, or a reversible PA-FP. Several proteins, like PA-GFP, Kaede, mEos, and Dronpa, have been used to tag different proteins to track them under different physiological conditions.¹¹⁷ They will also be useful in activating fluorescence of labeled proteins in MPS.

Aptamers are small single-stranded RNA or DNA oligonucleotides that bind to target molecules.¹¹⁸ The use of aptamers is similar to antibodies, without the toxicity and immunogenicity.¹¹⁸ Recently, aptamers were used in an in-line sensor to detect liver injury-mediated TGF β signaling.¹¹⁹

Nanoparticles (NP) have been applied to a variety of biomedical detection challenges, as well as a vehicle for delivery of therapeutics.¹²⁰ For example, an FITC-labeled anti-ICAM-1/NP has been used in an MPS to detect the effect of shear stress on the uptake in endothelial cells with TNF- α containing culture medium.¹²¹ Similarly, labeled nanoparticles have been used to visualize and to quantify intracellular oxygen and pH levels.¹²² A recent review explores fluorescent NPs as sensors for several bio-analytic molecules in different biological processes.¹²³

Fluorescent cyclic peptides have been used as a chemical scaffold for various imaging processes. These fluorescently labeled peptides have been used to detect apoptotic bodies¹²⁴ and drug-induced apoptosis in fixed or living cells.¹²⁵ A recent review describes a range of cyclic peptide designs and applications both for *in vitro* and *in vivo* applications.¹²⁶

Fluorescent probes are chemical dyes that can be diffused into cells. For example, intracellular lipid droplets can be detected with specificity by various photostable fluorescent chemicals, like Sudan III, Oil Red O, Nile red, and BODIPY.¹²⁷ Similarly, Lipid Toxtm, a neutral lipid stain, is used to detect and characterize the accumulation of neutral lipid.¹²⁷ Mito-ID intracellular probe can be used for direct measurements of intracellular oxygen concentration.¹²⁸ ROS-ID total ROS/superoxide can be used to distinguish different reactive species, such as hydrogen peroxide, peroxy nitrile, and hydroxy radicals.¹²⁹ However, fluorescent probes diffused into multi-cellular MPS will label all of the cells and are often either packaged by the cells or leak out over time. Nevertheless, some are valuable for short-term studies.¹²⁷

Challenges for recapitulating the progression of metabolic syndrome/MAFLD in human biomimetic liver MPS

There are many challenges to fully recapitulate the progression of MAFLD in human biomimetic liver MPS.³ Here we will focus on cells, 3D structural organization and function within the liver acinus MPS, media, measurements of key liver functions, and the ability to image the live system during the study.

The ultimate goal is to have fully matured, adult genotype, and phenotype consistent iPSC-derived cells that form the liver acinus including hepatocytes, cholangiocytes, stellate cells, Kupffer cells, and liver sinusoidal endothelial cells (LSECs), all from the same either healthy or disease-staged patient.^{3,60} However, at this time, the field continues to optimize iPSC-derived liver cells (e.g. hepatocytes).^{62,130-133} Success here will create an unlimited supply of isogenic cells from subpopulations of patients with distinct genotypes and status of disease (e.g. healthy or MAFLD). Until iPSC-derived cells have been optimized, we are now focused on using human primary cells for all the cell types, although this is also challenging. Fortunately, a number of suppliers are making human primary cells available, though isogenic sets of the four primary cell types still have limited availability. As a bridge to the use of either isogenic primary cells or all iPSC-derived cells, we

and others use a combination of primary hepatocytes and LSECs from the same patient, supplemented with well characterized human cell lines for stellate cells (e.g. LX-2) and Kupffer cells (activated THP-1).^{38,39} However, it will be important to replace the cell lines with isogenic primary cells or iPSC-derived cells, since the cell lines have been optimized to grow in culture and probably only partially reflect the performance of primary cells. In our present studies, we start with primary hepatocytes and LSECs from patients that exhibit NAFL, but not more advanced MAFLD based on pathology, and progress the disease with designed media. However, we have also performed studies using freshly isolated hepatocytes from patients diagnosed with more advanced MAFLD. We have found that freshly isolated hepatocytes with advanced disease are able to attach better than cryopreserved cells from patients with advanced disease. The addition of bile ducts with the inclusion of cholangiocytes is also an important challenge^{134,135} and a project in progress.⁶⁰

Our goal has been to create, as closely as possible, a fully human biomimetic liver MPS through the evolution of the experimental human liver MPS models.^{3,38,39,51} The concept is that recapitulating the liver acinus structure in 3D will optimize the functions of the MPS based on physical cell contacts, cell-cell communications, communication of factors and cells between the vascular channel (see Figure 2) and the hepatic channel, as well as cell migrations and proliferations (e.g. activated stellate cells). The important roles of the biochemistry and stiffness of the specific matrix materials that the cells are in are not discussed here, but is another challenge.^{3,52}

The content and flow rate of the media in the human biomimetic liver MPS are a challenge, especially for the formulation of media that will support the progression of the disease from a normal fasting (NF) state, to the progression through early metabolic syndrome (MAFLD) to late metabolic syndrome (T2D) over a two-week period (Table 2). We developed our initial media with glucose-free Williams E media supplemented with physiologically relevant levels of high and low glucose, insulin, glucagon, oleic acid, palmitic acid, and molecular drivers of disease including TGF- β and LPS.⁶⁴⁻⁶⁹ We then adjusted these components to reflect the pathophysiological conditions. We started with primary human hepatocytes from slightly steatotic (NAFL or MAFL) patients and matching patient LSECs along with well-characterized human cell lines for stellate and Kupffer cells. It is important to note that the media will continue to evolve to more closely reflect the key physiological/pathophysiological components found in patient blood.

It is important to measure a wide range of parameters in both the normal and disease state human biomimetic liver MPS over the time course of each study (typically 10-14 days). These include monitoring key components of the secretome, several FPBs (Table 1), additional imaging metrics, and fixed endpoint metrics (Table 3). All of these metrics are valuable in defining the temporal changes in the MPS during disease progression.³ Importantly, as MPS models and biomarkers evolve, we are evaluating other important metrics (ex. glutamate dehydrogenase as a

Table 3. Example phenotypic, functional, and genomic metrics of biomimetic MPS for liver metabolic syndrome disease models.

Readout	MPS live measurements	Clinical relevance
Secretome		
Albumin secretion	ELISA ⁵¹	Metabolic competence, overall hepatocyte function
Urea secretion	Colorimetric ⁵¹	Metabolic competence, overall hepatocyte function
LDH release ^a	Colorimetric ⁵¹	Hepatocellular injury corresponding with ALT and AST
Glucose secretion	AmplexRed glucose assay ¹³⁶	Glucose regulation
β -hydroxybutyrate	Colorimetric ¹³⁷	Fatty acid oxidation
Lactate secretion	Colorimetric ¹³⁸	Glycolysis
Cytokine release	Human cytokine panel ¹³⁹	Liver stress/injury response
Fatty acid secretion	Mass spectroscopy ¹⁴⁰	Fatty acid metabolism
TNF α secretion	ELISA ⁵¹	Kupffer activation, innate inflammatory response
Bile acids (BA)	BA profile by mass spectroscopy ¹⁴¹	NAFLD, NASH altered plasma BA profile corresponds
Exosomes (proteins/RNA/microRNA)	antibody (α -SK1), qRT-PCR ¹⁴²	Circulating extracellular vesicles containing SK1, miRNA-122 & -21 as markers for NAFLD, NASH, HCC
Fluorescent protein biosensors (FPBs)		
Hepatocyte apoptosis	Biosensor ^{4,51}	Hepatocellular injury/death
ROS (hepatocytes and Kupffer)	Biosensor ^{4,51}	Hepatocellular injury, Kupffer cell activation
Insulin resistance (hepatocytes)	Biosensor ^{143,144}	Lost suppression of glucose production
Cell tracking (stellate and Kupffer)	Biosensor ⁴	Morphology of early liver injury, proliferation
Additional FPBs	See Table 1	See Table 1
Additional imaging		
Steatosis	Brightfield & LipidTox ³⁸	Normal and/or pathological fat storage in hepatocytes
PMN infiltration	Imaging labeled PMNs ¹⁴⁵	Adaptive inflammatory response
Mitochondrial function	TMRE ³⁸	Hepatocellular health and function
Glucose uptake	6-NBDG ¹⁴⁶	Hepatocellular insulin resistance marker
Endpoint measurements		
Hepatocyte ballooning	Cytokeratin, anti-CK8/18	A key indication of NASH ¹⁴⁷
LSEC activation	ICAM antibody – IF ¹⁴⁸	Regulates fibrosis and inflammation responses
Fibrosis (stellate activation and collagen synthesis)	α -SMA, COL1A2 IF ⁵¹	Early fibrosis indicator and direct measure of fibrosis
RNAseq	RNA sequencing, multiple methods ¹⁴⁹	Comparison to patient results ^{8,150}

α -SK1: sphingosine kinase 1; α -SMA: alpha smooth muscle actin; COL1A2: collagen type 1A2.

^aBased on known clinical data.

liver-specific biomarker of hepatocellular damage^{151,152}) that inform disease progression. The central role played by FPBs, needed for real-time, temporal-spatial measurements, requires that the MPS can be directly imaged.

Status of quantifying the progression of metabolic syndrome in human biomimetic MPS

Important early human MPS models of disease progression of MAFLD/NASH demonstrated the ability to quantify a variety of metrics to define the disease state and to test potential therapeutics to halt or reverse MAFLD/NASH^{3,37,40,41,153–159}. Together with data from these published MPS models,^{3,37,40} some of the data shown below and some unpublished results, we are beginning to map the progression of the metabolic syndrome in the liver (Figure 5). Genetic predisposition and/or dietary intake of high fat and sugar-enriched foods can induce the progression from a “healthy” liver to the obese pre-diabetic MAFLD state and subsequently to a morbid NASH/T2D diabetic state. It has been demonstrated that NAFLD progression is a liver indicator of T2D in up to 70% of T2D patients.¹⁶⁰ Simulating these conditions in the human biomimetic liver MPS (LAMPS and vLAMPS) will help reveal

mechanistic insights into the progression of metabolic syndrome/MAFLD and potential therapeutic strategies. Clinically relevant stages of metabolic syndrome can be recapitulated in the LAMPS (where zone 1 and zone 3 are created in separate chips³⁸) and/or in the vLAMPS (where zonation is generated within a single chip³⁹) and metabolic changes are induced and maintained by the associated media formulations NF, EMS, or LMS (Figure 5(a)). We designed these media to recreate disease progression from Healthy/Normal Fasting (NF) to early metabolic syndrome (EMS or MAFLD) and late metabolic syndrome (LMS or NASH/T2D) over two weeks in LAMPS or vLAMPS (see Table 2).^{64–69} Figure 5(b) illustrates the experimental sequence used to induce selected metabolic changes associated with the progression from Healthy to MAFLD and then to NASH/T2D as demonstrated in multiple liver MPS.^{3,37–41} In the NF condition, the four cell-type LAMPS and/or vLAMPS show a peak secretion of albumin at five to seven days. Progressive MAFLD and NASH/T2D states exhibit critical phenotypes of metabolic syndrome: hepatic steatosis, oxidative stress, inflammatory cytokines, stellate cell activation and proliferation, hepatic ballooning, fibrosis, and ultimately hepatic insulin resistance (manuscript in preparation). Measurements of these phenotypes are consistent with clinical data.^{161–164}

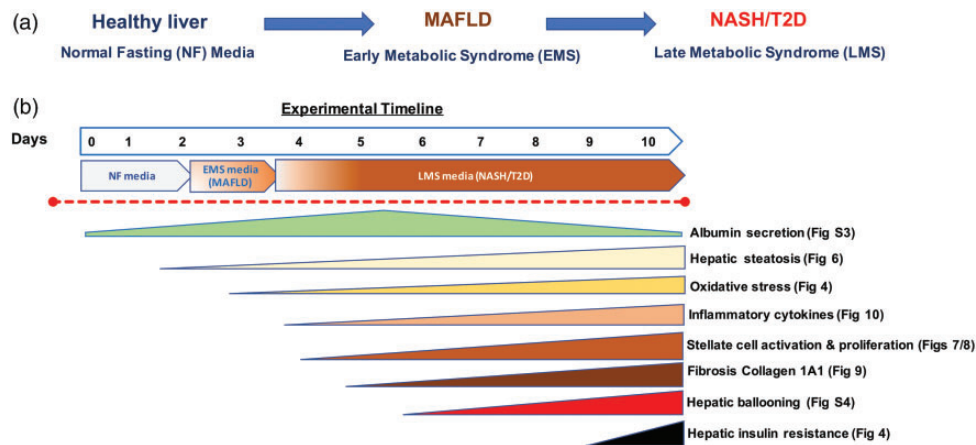


Figure 5. Modeling the clinically relevant stages of metabolic syndrome using liver MPS. (a) Metabolic syndrome/MAFLD is characterized by a progression from a healthy liver towards a MAFLD state and subsequently to a NASH/T2D state. To track the progression of metabolic syndrome in a liver MPS, we simulate these conditions with three media formulations: NF, EMS, and LMS (Table 2). (b) Description of the experimental timeline used to mimic disease progression from the normal healthy liver to early metabolic syndrome (EMS; MAFLD) and then late metabolic syndrome (LMS; NASH/T2D) over a two-week period. Progression is monitored with a set of clinically relevant biomarkers^{117–120} (Table 3) critical to the characterization of metabolic syndrome progression. Bars show the approximate timing of the onset and increase in biomarker signals.

As shown in Figure S3, LAMPS secretome measurements demonstrate that EMS and LMS media treatments result in different albumin (ALB), blood urea nitrogen (BUN), and lactate dehydrogenase (LDH) secretion profiles compared to NF conditions. Efflux samples were collected at days 2, 4, 6, 8, and 10 of the experimental time course and levels of ALB (Figure S3(a)), BUN (Figure S3(b)), and LDH (Figure S3(c)) were quantified for LAMPS maintained at either zone 1 or zone 3 flow conditions. Significant decreases in ALB and BUN were observed at various time points in LAMPS maintained in NF, EMS, and LMS media under either zone 1 or zone 3 flow conditions, consistent with previous reports.^{37,153,165–169} A statistical summary of these comparisons is shown in Table S2. Similar to our previous work in LAMPS,³⁸ decreased ALB and BUN production are also observed in zone 3 models compared to zone 1 groups. Treatment with EMS and LMS media results in significantly increased LDH secretion over the 10-day time course in Zone 3 LAMPS, as reported in other studies.¹⁷⁰ A similar trend was observed in Zone 1 LAMPS but was not statistically significant. These results suggest that both EMS and LMS media treatments result in secretion profiles that are consistent with both *in vitro* and clinical studies, demonstrating the disease progression of the metabolic syndrome.^{165–170} In addition to these basic secretome efflux measurements, more extensive secretome measurements were made to examine differences in the secretion of various cytokines (Table S3), as discussed below.

We next examined whether our experimental media conditions in LAMPS could induce the lipid accumulation phenotype associated with the progression of metabolic syndrome. Figure 6 demonstrates that either EMS or LMS media treatment results in increased steatosis in hepatocytes compared to NF media. As shown qualitatively, both bright field and LipidTOX (red) image fields from LAMPS treated with NF, EMS, or LMS media for 10 days in either Zone 1 or Zone 3 results in increased lipid accumulation compared to NF media in the same zone (Figure 6

(a)). We next quantified the hepatic steatosis observed in the LAMPS models. As shown in Figure 6(b) and (c), significant increases in the integrated intensity of lipid droplet fluorescence are observed for both microvesicular steatosis ($<125 \mu\text{m}^2$) and macrovesicular steatosis ($>125 \mu\text{m}^2$) measured in LAMPS maintained in either EMS or LMS media compared to NF media. Moreover, we demonstrate that there is significantly more lipid accumulated in the LMS media condition compared to the EMS media treatment, and this difference is observed for both microvesicular and macrovesicular steatosis lipid droplet subpopulations in either zone. In addition, zone-specific increases in steatosis are observed between NF, EMS, and LMS media groups as well as in Zone 3 (blue bars) compared to Zone 1 (red bars) within each media condition (Figure 6(d) and (e)). These results demonstrate that in all media treatments, there is greater accumulation of lipid droplets in Zone 3 compared to Zone 1, consistent with our previous work.³⁸ Taken together, these data provide evidence that both metabolic syndrome disease medias mimic conditions of disease progression when compared to the normal fasting state and are consistent with lipid accumulation phenotypes observed in other MPS models.^{37,40}

We next examined hepatocyte ballooning, another key metric in defining disease progression,^{147,171} by immunofluorescence staining of cytokeratin-18 (CK-18) in hepatocytes. Figure S4(a) shows representative images from LAMPS models treated with NF, EMS, or LMS media and labeled with anti-CK-18. Both EMS and LMS media treatments induced hepatocyte ballooning indicated by disruption of hepatocyte CK-18 organization, statistically significant increase in cellular area (Figure S4(b)), accumulation of peripheral CK-18 (white arrowheads), appearance of Mallory-Denk body-like structures (yellow arrowheads), and nuclei pushed to the periphery (orange arrowheads). In LMS-treated models, late-stage hepatocyte injury is evident from the appearance of apoptotic nuclei (red arrow), while normal hepatocellular size and CK-18 organization is

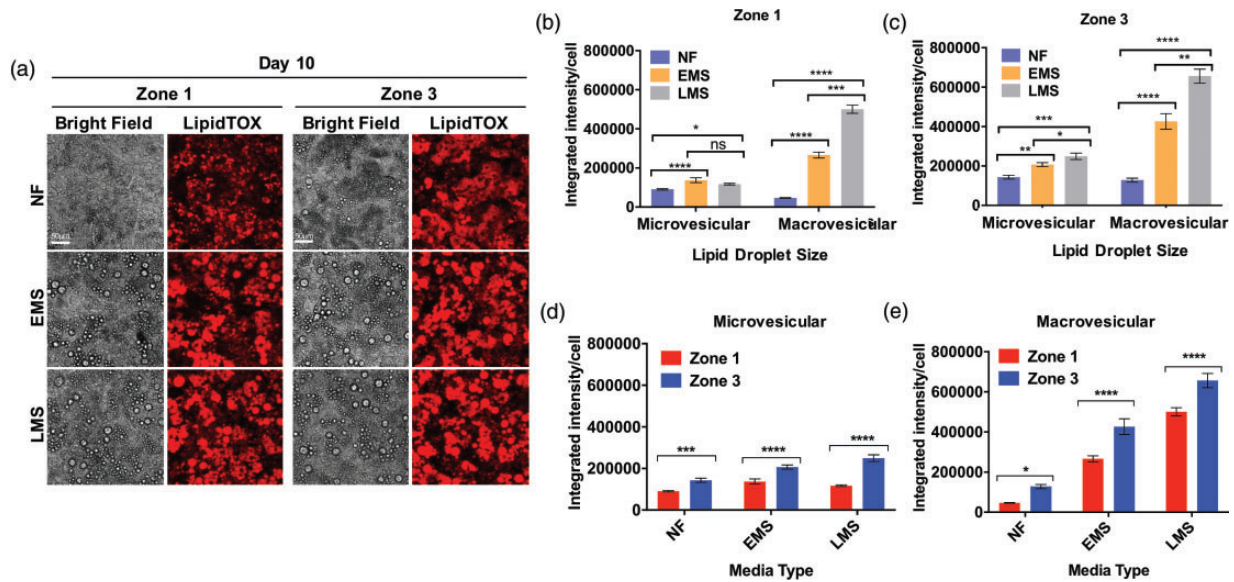


Figure 6. EMS and LMS media treatment results in increased steatosis in hepatocytes compared to normal fasting media. (a) Representative Day 10 bright field (gray) and LipidTOX (red) images of LAMPS treated with NF, EMS, LMS media in either Zone 1 or Zone 3 (Images were acquired with a 20 \times (0.45 NA) objective; Scale bar: 50 μm). (b–e) Quantitation of hepatic steatosis (LipidTOX) in day 10 LAMPS models. (b–c) Significant increases in the lipid droplet integrated intensity for both microvesicular steatosis (droplet area $< 125 \mu\text{m}^2$) and macrovesicular steatosis (droplet area $> 125 \mu\text{m}^2$) is seen in Zone 1 (b) and Zone 3 (c) LAMPS maintained in either EMS or LMS media compared to NF media. (d–e) Significant increases in lipid droplet integrated intensity are observed for both micro- (d) and macrovesicular steatosis (e) in Zone 3 (blue bars) compared to Zone 1 (red bars) in each media condition, consistent with our previous work.³⁸ Twenty-four fields from $n = 3$ chips were analyzed for each media/zone. Statistical significance was assessed using a one-way ANOVA with multiple comparisons (Tukey Test: * $P < 0.05$; ** $P < 0.01$; *** $P < 0.001$; **** $P < 0.0001$).

found in NF media treated control. Overall, both the observed increase in lipid accumulation and stellate cell activation, as well as hepatocyte ballooning demonstrate that both EMS and LMS media treatments recapitulate key steps in the progression of metabolic syndrome towards fibrosis.

As metabolic syndrome progresses, stellate cells in the liver emerge from a quiescent state into an activated myofibroblast-like state leading to the fibrotic cascade associated with disease progression.¹⁷² The main phenotypic marker of stellate cell activation is the expression of α -smooth muscle actin (α -SMA). Therefore, we examined stellate cell activation by immunofluorescence staining of α -SMA in LAMPS treated with our different media. As shown in Figure 7(a), representative Day 10 bright field, Hoechst (blue), and α -SMA (red) image fields from LAMPS treated with NF, EMS, or LMS media in either Zone 1 or Zone 3 show that both EMS and LMS media treatment result in increased α -SMA expression (myofibroblast-like phenotype) by LX-2 stellate cells compared to NF in either zone, suggesting that either disease media treatment results in increased stellate cell activation. Qualitatively, there is also an increase in the number of activated stellate cells in the LAMPS treated with EMS and LMS compared with NF in zones 1 and 3. In contrast, less stellate cell activation is observed in devices maintained with NF media, consistent with more quiescent stellate cells in the normal fasting state. Quantitatively, a significant increase in α -SMA integrated intensity is observed between either EMS or LMS media compared to NF media in either Zone 1 (Figure 7(b)) or Zone 3 (Figure 7(c)) LAMPS. Furthermore, there is a significant increase in

α -SMA integrated intensity in LMS media compared to EMS, indicating a higher level of stellate cell activation in LMS-treated models. In addition, as shown in Figure 7(d), zone-specific quantitation of α -SMA expression in LAMPS shows that a significant increase in α -SMA intensity is observed in Zone 3 (blue bars) compared to Zone 1 (red bars) in both EMS and LMS media, while no zone-specific differences are observed in NF media treatment groups.

As a result of the qualitative observation of the increase in the number of activated stellate cells in LAMPS treated with EMS and LMS, we used an FPB to quantify stellate cell proliferation in EMS and LMS media conditions, as increased proliferation has been demonstrated to be a key part of the overall activation of stellate cells in the fibrotic response.^{40,41,172} One of the key features of the LAMPS model is its effectiveness for live imaging in conjunction with biosensor technologies. Histone 2B (H2B)-FusionRed-expressing LX-2 cells were used to track the proliferation of stellate cells in LAMPS models maintained in either EMS, or LMS media over a 10-day time course. Representative images at day 10 in zone 3 demonstrate a greater number of LX-2 nuclei in LMS-treated LAMPS compared to those treated with EMS media (Figure 8(a)). Furthermore, the number of LX-2 nuclei was quantified, and LAMPS maintained in LMS media demonstrate a significant increase in proliferation at day 10 compared to EMS-treated models in zone 3 (Figure 8(b)). The difference in proliferation between EMS and LMS suggests that the presence of TGF- β in LMS media drives an increase in proliferation, consistent with its known role as a driver of stellate cell activation/proliferation in the disease process.^{173,174}

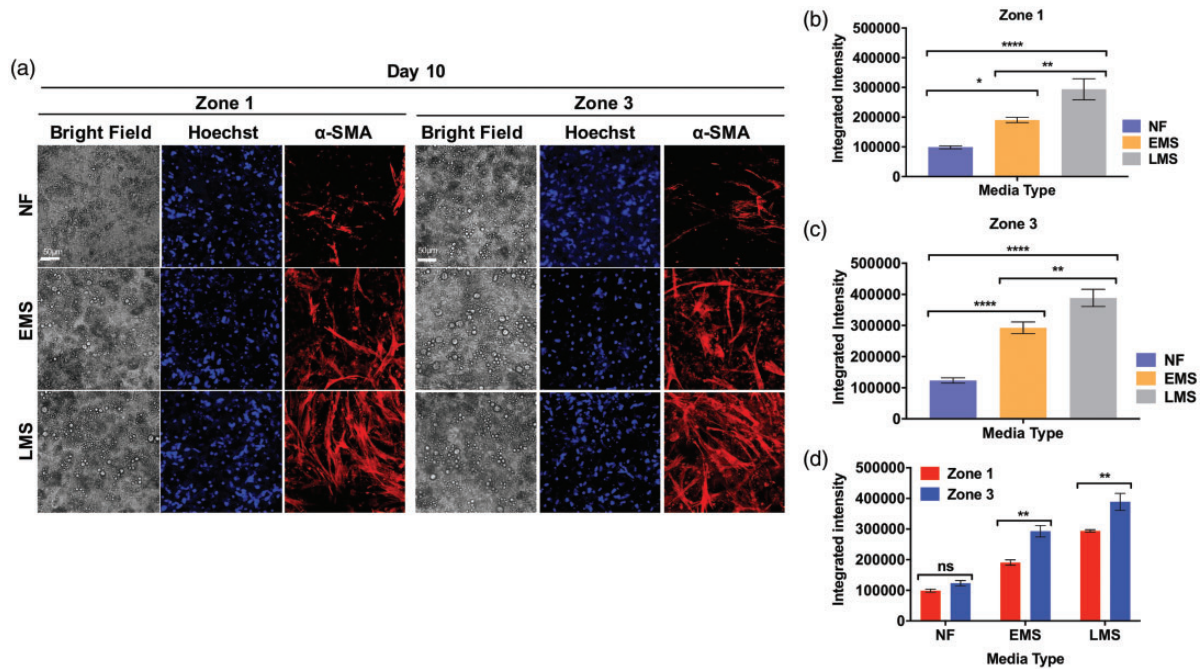


Figure 7. EMS and LMS media treatment results in increased α -SMA expression in stellate cells compared to normal fasting media. (a) Representative Day 10 bright field (gray), Hoechst (blue), and α -SMA (red) images of LAMPS treated with NF, EMS, LMS media in either Zone 1 or Zone 3 (Images were acquired with a 20 \times (0.45 NA) objective; Scale bar: 50 μ m). (b–c) Quantitation of α -SMA expression in day 10 LAMPS models. Significant increases in α -SMA integrated intensity are observed between both EMS and LMS compared to NF in Zone 1 (b) or Zone 3 (c). Additionally, there is also a qualitative increase in the number of activated stellate cells in the LAMPS treated with EMS and LMS compared with NF. (d) α -SMA intensity also significantly increased in Zone 3 (blue bars) compared to Zone 1 (red bars) in both EMS and LMS media, while no difference is observed in NF media. For each media condition, 24 fields from $n = 3$ chips were analyzed. Statistical significance was assessed using a one-way ANOVA with multiple comparisons (Tukey Test: * $P < 0.05$; ** $P < 0.01$; *** $P < 0.001$; **** $P < 0.0001$).

A critical aspect of using a localization FBS in LX-2 cells (and primary or iPSC-derived stellates in the near future) in biomimetic liver MPS is that it allows for the monitoring and quantification of the spatial distribution of stellate cells throughout the experimental time course. To demonstrate this capability, individual YZ projections of H2B-FusionRed LX-2 cell distributions in LAMPS through time (days 1, 5, 10) were created for each media (NF, EMS, LMS) and each zonation condition (zone 1 and zone 3), to explore the spatial-temporal phenotypes conferred by these distributions (Figure S5). On day 1, the stellate cells can be found throughout the entire Z range ($\sim 800 \mu\text{m}$), while at later time points (day 5 and 10), the stellate cells are found in close proximity to the hepatocyte layer, near the bottom of the Z section (Figure S5(a)). The quantitation of the intensity distributions through the z-range (Figure S5(b)) supports this conclusion, as increased fluorescence intensity is observed on Day 1 in the higher Z-distance range (150 μm –400 μm) compared to intensity values observed in Days 5 and 10 in the same region. On Days 5 and 10, intensity values are confined to the lower portion of the Z-range (0–150 μm and 0–200 μm respectively) indicating that while LX-2 cells are initially suspended in the collagen matrix overlay, at later time points the majority of LX-2 cells are located near the hepatocytes. We observed a similar Z-distribution of LX-2 cells across each of the media and zone conditions tested. Taken together, we have shown that the H2B-FusionRed localization FPB can be used to both track the proliferation and characterize the relative z-position of LX-2 cells within LAMPS models.

While these observations clearly demonstrate the usefulness of employing localization FPBs in MPS models to define temporal and spatial relationships of stellate cells to the hepatocytes, it is important to note the limitation that these results do not provide insight into the underlying mechanisms that drive LX-2 proliferation and localization in LAMPS. For example, our results show that while LX-2 cells are more evenly distributed throughout the collagen matrix in the LAMPS model at early time points, over time these cells become more concentrated in an area in close proximity to the hepatocyte layer. However, this particular biosensor does not reveal whether the LX-2 cells in our model are migrating towards the hepatocyte layer due to a specific signaling event or whether changes in the physical properties of the collagen matrix (e.g. concentration, stiffness etc.) over time facilitate the movement of LX-2 cells to a closer proximity to the hepatocytes, or perhaps the cells proliferate in proximity to the hepatocytes and undergo necrosis in the collagen gel. Here, the use of additional metrics, increased time resolution and experimental manipulation of the cell content and matrix composition and stiffness, will be required to provide additional mechanistic insights. However, this is a key value of harnessing FPBs and human biomimetic liver MPS, since the contents and characteristics can be investigated.³

To determine if our disease model provides evidence of increased fibrosis, we used immunofluorescence labeling to examine the secretion of the pro-fibrotic markers collagen 1A1 (Figure 9(a)) and TIMP-1 (Figure 9(b))^{37,173,175} on day 10 in LAMPS models treated with EMS and LMS media and

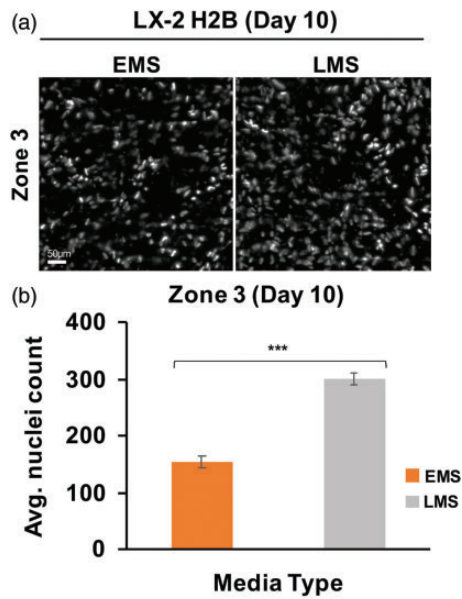


Figure 8. LMS media treatment results in increased stellate cell proliferation compared to EMS media treatment. (a) Representative Day 10 images of H2B-FusionRed LX-2 nuclei in LAMPS treated with EMS or LMS media in Zone 3. (Images were acquired with a 20× (0.45 NA) objective; Scale bar: 50 μm). (b) Quantitation of LX-2 cell proliferation in Zone 3 LAMPS at day 10. LAMPS maintained in LMS media show increased proliferation compared to EMS media. The difference in proliferation between EMS and LMS suggests that the presence of TGF-β in LMS media drives an increase in proliferation, consistent with its known role as a driver of stellate cell activation/proliferation in disease progression. For each media condition, six fields from $n = 2$ chips were analyzed. Statistical significance was assessed using an unpaired, two-tailed *t*-test to compare EMS and LMS media groups (***) $P < 0.001$. Z-axis projections and intensity distributions of LX-2 cells in LAMPS across zone and media type are shown in Figure S5.

maintained at either Zone 1 or Zone 3. For collagen 1A1, significant increases were observed between NF media and both EMS and LMS media in both zone 1 and zone 3 (Figure 9(a)). While a significant increase in TIMP-1 secretion was observed for EMS and LMS in zone 3, a significant increase in TIMP-1 was observed only in the EMS media condition in zone 1 (Figure 9(b)). In addition, we observed an apparent increase in extracellular collagen 1A1 deposition around the periphery of LX-2 cells (indicated as a diffuse fluorescence surrounding the cells) in LAMPS treated with either EMS or LMS media compared to NF treatment (Figure 9(c)), consistent with the efflux results described above and indicating an increase of collagen 1A1 in models treated with EMS and LMS media compared to NF media. These results are consistent with findings presented in other liver MPS systems identifying phenotypic markers of NAFLD progression^{37,40,41,154} and suggest that our model system also promotes fibrosis, a key factor in the development of metabolic syndrome.

As inflammation is one of the main drivers of metabolic syndrome disease progression towards fibrosis, we examined if there were differences in the secretion of a selected panel of cytokines in LAMPS treated with EMS and LMS media compared to those in NF media. Efflux samples were collected at Day 10 and individual cytokine secretion profiles for each media condition and zone were generated using the R&D Systems Human XL Discovery Panel, a

multiplex Luminex[®] assay consisting of 45 targets including cytokines, chemokines, and growth factors (Figure 10 and Table S3). Figure 10 shows the cytokines within each media treatment and zone group that were significantly increased or decreased compared to NF media values (P -value < 0.05). The cytokine panel secretion profiles demonstrate unique signatures for both EMS and LMS media. In zone 1, only a small number of cytokines were significantly changed compared to NF media (Figure 10(a) and (b)), most notably the pro-inflammatory cytokine IL-6 was significantly increased only in the LMS media condition, which contains both pro-inflammatory (LPS) and pro-fibrotic (TGF-β) drivers not included in the EMS media formulation. The increase in IL-6 levels in LMS-treated LAMPS is consistent with both the observation that LPS induces the production of IL-6 and with the role of TGF-β as a key mediator in stellate cell activation resulting in the progression towards hepatic fibrosis.^{24,176–180}

For a much larger subset of cytokines, secretion in zone 3 was significantly increased for both EMS and LMS media treatments, consistent with previous histological characterizations demonstrating that fibrosis in NAFLD/NASH is predominant in zone 3.^{181,182} While the EMS media group (Figure 10(c)) had 17 significantly increased cytokines, the LMS media group (Figure 10(d)) had 19 significantly increased cytokines, with 15 that were found in common between the media groups. Table S3 summarizes these findings and provides a detailed reference list for the described role of each of these cytokines in the progression of metabolic syndrome. The cytokine profiles from zone 3 LAMPS observed in the EMS and LMS media groups are consistent with the cytokine secretion profiles obtained by other groups using lipotoxic and/or fibrogenic media formulations in liver MPS models containing stellate and Kupffer cells.^{37,40,153,154} However, it is important to note that despite this overall similarity, each of these MPS platforms employed different media conditions and cell sources. Thus, as liver MPS platforms continue to evolve, this highlights the need to drive towards employing a more common set of standard normal and disease media formulations as well as common iPSC and primary cell sources, so that comparisons between MPS platforms are more straightforward. Several pro-inflammatory cytokines increased in both EMS and LMS media treatments including IL-6, IL-8, IL-2, IL-1β, and TNF-α, which have all been implicated in the progression of metabolic syndrome and have been shown clinically to be upregulated in NAFLD/NASH patients, as well as in multiple *in vitro* and animal studies.^{24,179,183–185} In addition, our results demonstrate an increase in factors linked to the activation and proliferation of stellate cells. Significant increases were observed in EMS and LMS media conditions for both PDGF and VEGF, growth factors that are critical for the proliferation of hepatic stellate cells,¹⁷² as well as increased levels of IL-33, which has been shown to drive hepatic fibrosis through activation of hepatic stellate cells.¹⁸⁶ Finally, our data demonstrate an increase in IL-15, a cytokine that has been documented to have pleiotropic effects in the progression of liver fibrosis.^{172,187,188} For example, in one murine model, IL-15 was shown to have a protective function in the fibrogenic

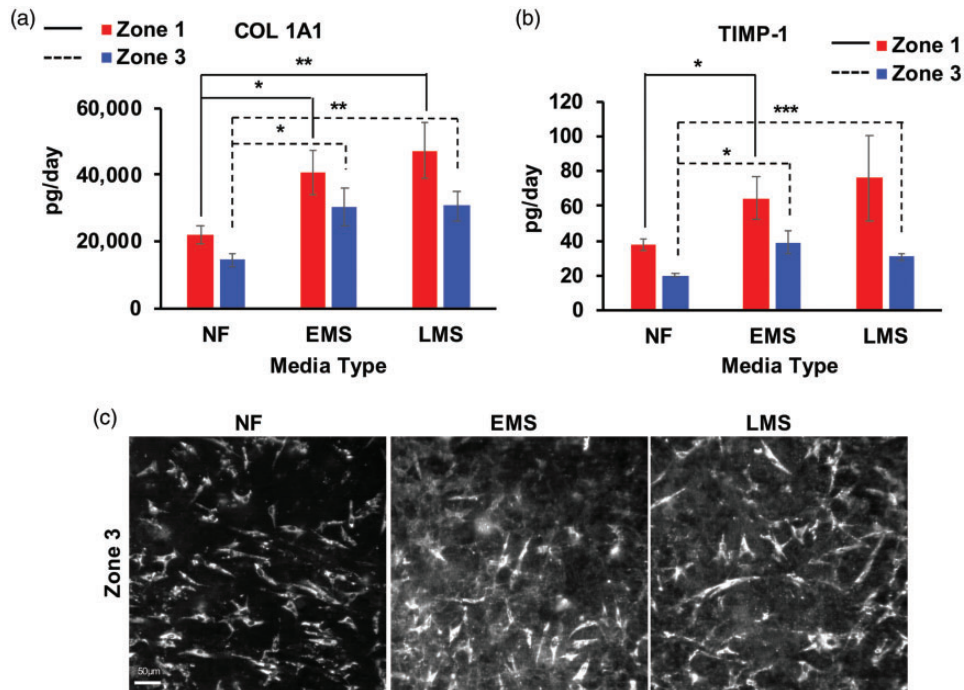


Figure 9. EMS and LMS media result in increased secretion of collagen 1A1 and TIMP-1. Efflux samples were collected at day 10 to detect levels of collagen 1A1 and TIMP-1 in LAMPS treated with NF, EMS, or LMS media in zone 1 or zone 3. (a) A significant increase in collagen 1A1 secretion was observed for both EMS and LMS relative to NF in both zone 1 and zone 3. (b) A significant increase in TIMP-1 secretion was observed for EMS and LMS relative to NF in zone 3, while only for EMS in zone 1. For each media condition, efflux from $n = 10$ chips was analyzed and statistical significance was assessed using a one-way ANOVA with multiple comparisons (Tukey Test $*P < 0.05$; $**P < 0.01$; $***P < 0.001$; $****P < 0.0001$). (c) Representative Day 10 images of LAMPS treated with NF, EMS, or LMS media in Zone 3 demonstrate that both EMS and LMS media treatment resulted in increased collagen 1A1 secretion compared to NF. Scale bar: 100 μm .

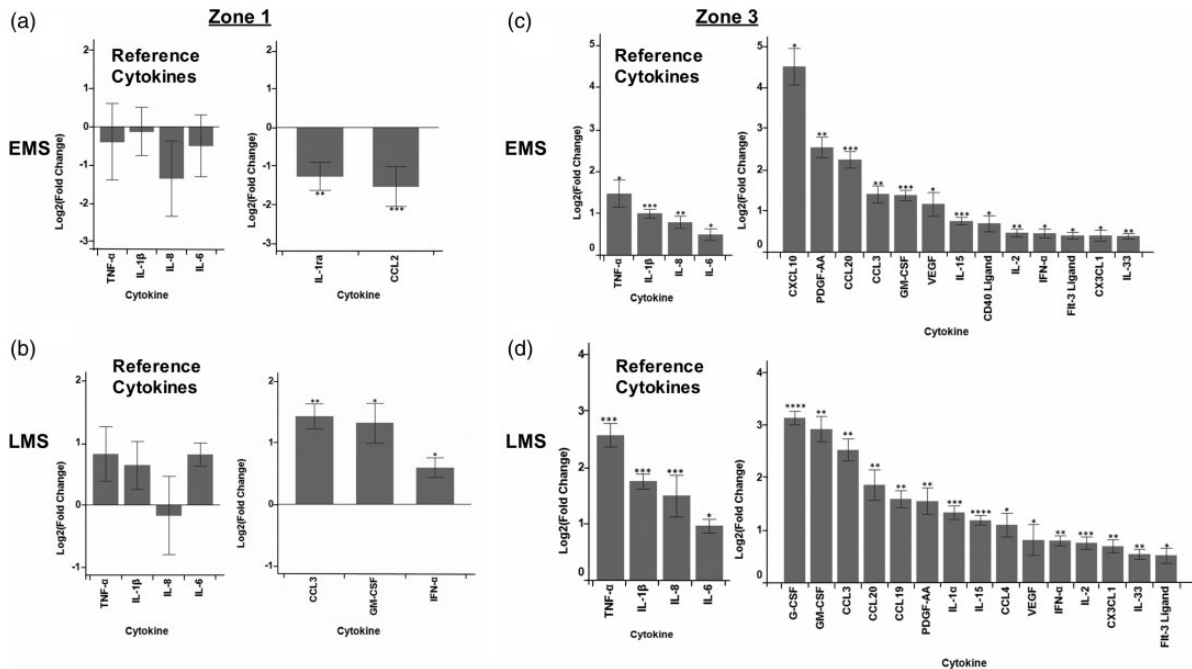


Figure 10. Cytokine panel secretion profiles demonstrate unique signatures for EMS and LMS media compared to NF. Efflux samples were collected at day 10 from LAMPS models treated with NF, EMS, or LMS media maintained at either zone 1 or zone 3. Individual cytokine secretion profiles for each media/zone condition were generated using the R&D Systems Human XL Discovery Panel. The data are displayed as the average log₂ (fold change) compared to NF media for both EMS (a and c) and LMS (b and d) in both zone 1 and zone 3. A total of $n = 6-7$ LAMPS were analyzed for each media/zone condition. Displayed are the cytokines within each media group that were significantly increased or decreased compared to NF. The reference cytokine designation highlights specific pro-inflammatory cytokines commonly associated with MAFLD/NASH disease progression (TNF- α , IL-1 β , IL-8, and IL-6) that were significantly increased in both EMS and LMS media treatments. Statistical significance for individual cytokines was assessed using a two-tailed t -test ($*P < .05$; $**P < .001$; $***P < .0001$; $****P < .00001$). Table S3 provides a detailed reference list for the potential role of each of these cytokines in metabolic syndrome progression.

response by modulating collagen mRNA expression in stellate cells where *IL-15R α* knockout mice displayed an increase in collagen production.¹⁸⁷ In contrast, using a mouse model of steatohepatitis induced by a high-fat diet, it was shown that activated stellate cells produce granulocyte-macrophage colony-stimulating factor (GM-CSF) and IL-15 to enhance survival of neutrophils promoting liver fibrosis.¹⁸⁸ Consistent with the latter study, we also observed a significant increase in GM-CSF production along with IL-15 in both EMS and LMS media treatments. Taken together, our cytokine profile data suggest that both EMS and LMS media types support an increased inflammatory response in LAMPS models. As described above, it is important to note that the formulations of our disease media will continue to evolve to more closely reflect physiological/pathophysiological components found in patient blood.

Perspectives on harnessing FPBs to quantify the progression of metabolic syndrome in human biomimetic MPS

FPBs are expected to provide key metrics for defining the temporal and spatial dynamics of specific pathophysiological parameters (e.g. changes in liver zonation) that track disease progression, and identify key biomarkers of disease progression and response to therapeutics. In a single MPS, up to three FPBs can be incorporated based on spectral selection of the fluorescent proteins used to construct the FPBs and their use in different cell types. This spectral multiplexing allows the correlation of temporal-spatial changes in key parameters in the same MPS (Table 1, Figure 5). Additionally, fluorescence lifetime measurements will allow more FPBs to be multiplexed.^{189,190} Computational exploration of genomics, including RNASeq data from patients, also is expected to yield additional molecular targets within additional key pathways that could be used for designing, constructing, and testing new FPBs. Upon the completed development of mature iPSC-derived parenchymal and non-parenchymal cells, it will be possible to use CRISPR to create FPB-cells for each patient/genomic background, which can be incorporated into patient-specific MPS. This will be a powerful platform for performing preclinical trial studies and precision medicine.³

There continue to be challenges in building and applying human biomimetic liver MPS to investigate mechanisms of disease progression and to perform drug discovery and development studies. We, and others, have discussed a few of these challenges.³ The field is moving forward and other major challenges including matrix biochemistry and stiffness,^{191,192} chip materials with low nonspecific binding,^{193,194} physiological scaling of the model,¹⁹⁵ robust and reproducible model performance,⁷ onboard sensors for biochemical readouts,¹⁹⁶⁻¹⁹⁸ and optimization of medium to support multiple cell types in a MPS are being addressed. The challenges are even greater when physically linking multiple organ MPS.^{195,199} Furthermore, human biomimetic liver MPS data must be compared to clinical parameters including patient blood parameters.

A great opportunity exists for combining FPBs, human biomimetic MPS, and the MPS-Db with QSP¹⁻³ to create a platform for drug repurposing and novel drug discovery, as well as the identification of biomarkers of disease progression and response to therapeutic treatments. The iterative computational and experimental approach of QSP allows an approach to drug discovery and development that is complementary to target-centric methods.¹

AUTHORS' CONTRIBUTIONS

Conceptualization: DLT, MM, AG, AS, LV; MPS experimentation and data analysis: MS, AJ, VM, DG, T-YS, RD, XL, CR, LV, MM, AG; Computational biology and QSP: DL, AS, AG, DLT; Strategic planning: AS-G, EK, V,Y, JB, LV, AS, AG, MM, DLT; Clinical perspective: EEK, VY, JB, AS-G, AS; Writing First Draft: MS, AJ, VM, MM; Full draft writing: Equal contributions, data and concept visualization: MM, AJ, DG, AG, DLT.

ACKNOWLEDGEMENTS

The authors would like to thank all members of their laboratories for supporting the research efforts reported here. The cytokine data presented here was obtained using the UPCI Cancer Biomarkers Facility: Luminex Core Laboratory.

DECLARATION OF CONFLICTING INTERESTS

The author(s) declared the following potential conflicts of interest with respect to the research, authorship, and/or publication of this article: A.S-G is a co-founder and D.L.T. is an advisor for Von Baer Wolff, Inc., a company focused on bio-fabrication of autologous human hepatocytes using stem cell technology and genetic reprogramming to overcome liver failure. Their interests are managed by the Conflict-of-Interest Office at the University of Pittsburgh, USA, in accordance with their policies. The other authors declared no potential conflicts of interest with respect to the research, authorship, and/or publication of this article.

FUNDING

The author(s) disclosed receipt of the following financial support for the research, authorship and/or publication of this article: Funding that supported this research included: 1UG3TR003289-01-NIH/NCATS (J. Behari, A.Soto-Gutierrez, DLTaylor, MPI's), 4UH3DK119973-03-NIH/NIDDK (Taylor PI), S10OD12269-NIH (Taylor, PI), U24TR002632-NIH/NCATS (M. Schurdak and A. Gough, MPI's), 5U01TR002383-03-NIH/NCATS (DL Taylor, J.Wikswow, W. Murphy PI's), R01 DK097160-NIH/NIDDK (V. Yechoor), General Electric, Gilead Sciences, Endra Sciences, Pfizer (J. Behari) and institutional research contracts with Gilead, Intercept, Enanta, Galmed, Genentech, Pfizer, Celgene and Galactin. This work was also supported by NIH grant 1P30DK120531-01 to Pittsburgh Liver Research Center (PLRC).

DATA AVAILABILITY

The datasets generated and analyzed during the current study are available from the corresponding author on reasonable request.

ORCID IDs

Manush Saydmohammed  <https://orcid.org/0000-0001-7850-0732>

Mark T Miedel  <https://orcid.org/0000-0002-0132-6032>

SUPPLEMENTAL MATERIAL

Supplemental material for this article is available online.

REFERENCES

- Stern AM, Schurdak ME, Bahar I, Berg JM, Taylor DL. A perspective on implementing a quantitative systems pharmacology platform for drug discovery and the advancement of personalized medicine. *J Biomol Screen* 2016;**21**:521–34
- Taylor DL, Gough A, Schurdak ME, Vernetti L, Chennubhotla CS, Lefever D, Pei F, Faeder JR, Lezon TR, Stern AM, Bahar I. Harnessing human microphysiology systems as key experimental models for quantitative systems pharmacology. *Handb Exp Pharmacol* 2019;**260**:327–67
- Gough A, Soto-Gutierrez A, Vernetti L, Ebrahimkhani MR, Stern AM, Taylor DL. Human biomimetic liver microphysiology systems in drug development and precision medicine. *Nat Rev Gastroenterol Hepatol* 2021;**18**:252–68
- Senutovitch N, Vernetti L, Boltz R, DeBiasio R, Gough A, Taylor DL. Fluorescent protein biosensors applied to microphysiological systems. *Exp Biol Med* 2015;**240**:795–808
- Giuliano KA, Post PL, Hahn KM, Taylor DL. Fluorescent protein biosensors: measurement of molecular dynamics in living cells. *Annu Rev Biophys Biomol Struct* 1995;**24**:405–34
- Bergenthal LM, Shun TY, Vernetti L, Taylor DL, Gough AH. The Microphysiology Systems Database, <http://mps.csb.pitt.edu> (2018, accessed 3 April 2021)
- Schurdak M, Vernetti L, Bergenthal L, Wolter QK, Shun TY, Karcher S, Taylor DL, Gough A. Applications of the microphysiology systems database for experimental ADME-Tox and disease models. *Lab Chip* 2020;**20**:1472–92
- Gerhard GS, Legendre C, Still CD, Chu X, Petrick A, DiStefano JK. Transcriptomic profiling of obesity-related nonalcoholic steatohepatitis reveals a core set of fibrosis-specific genes. *J Endocr Soc* 2018;**2**:710–26
- Pirola CJ, Sookoian S. Multiomics biomarkers for the prediction of nonalcoholic fatty liver disease severity. *World J Gastroenterol* 2018;**24**:1601–15
- Dumas ME, Kinross J, Nicholson JK. Metabolic phenotyping and systems biology approaches to understanding metabolic syndrome and fatty liver disease. *Gastroenterology* 2014;**146**:46–62
- Li L, Liu H, Hu X, Huang Y, Wang Y, He Y, Lei Q. Identification of key genes in nonalcoholic fatty liver disease progression based on bioinformatics analysis. *Mol Med Rep* 2018;**17**:7708–20
- Blencowe M, Karunanayake T, Wier J, Hsu N, Yang X. Network modeling approaches and applications to unravelling non-alcoholic fatty liver disease. *Genes* 2019;**10**:966
- Veyel D, Wenger K, Broermann A, Bretschneider T, Luippold AH, Krawczyk B, Rist W, Simon E. Biomarker discovery for chronic liver diseases by multi-omics – a preclinical case study. *Sci Rep* 2020;**10**:1314
- Misselbeck K, Parolo S, Lorenzini F, Savoca V, Leonardelli L, Bora P, Morine MJ, Mione MC, Domenici E, Priami C. A network-based approach to identify deregulated pathways and drug effects in metabolic syndrome. *Nat Commun* 2019;**10**:5215
- Sookoian S, Pirola CJ. Repurposing drugs to target nonalcoholic steatohepatitis. *World J Gastroenterol* 2019;**25**:1783–96
- Wooden B, Goossens N, Hoshida Y, Friedman SL. Using big data to discover diagnostics and therapeutics for gastrointestinal and liver diseases. *Gastroenterology* 2017;**152**:53–67.e3
- Mardinoglu A, Boren J, Smith U, Uhlen M, Nielsen J. Systems biology in hepatology: approaches and applications. *Nat Rev Gastroenterol Hepatol* 2018;**15**:365–77
- Lefever D, Pei F, Miedel MT, DiStefano J, Yechoor V, Monga P, Soto-Gutierrez A, Bataller R, Vernetti L, Bahar I, Gough A, Stern AM, Taylor DL. Integration of quantitative systems pharmacology and a human metabolic dysfunction associated fatty liver disease microphysiology system to predict and test drugs for repurposing. *Hepatology* 2021;in preparation
- Soto-Gutierrez A, Gough A, Vernetti LA, Taylor DL, Monga SP. Pre-clinical and clinical investigations of metabolic zonation in liver diseases: the potential of microphysiology systems. *Exp Biol Med* 2017;**242**:1605–16
- Saklayen MG. The global epidemic of the metabolic syndrome. *Curr Hypertens Rep* 2018;**20**:12
- Samson SL, Garber AJ. Metabolic syndrome. *Endocrinol Metab Clin North Am* 2014;**43**:1–23
- Sanyal AJ. Past, present and future perspectives in nonalcoholic fatty liver disease. *Nat Rev Gastroenterol Hepatol* 2019;**16**:377–86
- Kleinert M, Clemmensen C, Hofmann SM, Moore MC, Renner S, Woods SC, Huypens P, Beckers J, de Angelis MH, Schurmann A, Bakhti M, Klingenspor M, Heiman M, Cherrington AD, Ristow M, Lickert H, Wolf E, Havel PJ, Muller TD, Tschop MH. Animal models of obesity and diabetes mellitus. *Nat Rev Endocrinol* 2018;**14**:140–62
- Braunersreuther V, Viviani GL, Mach F, Montecucco F. Role of cytokines and chemokines in non-alcoholic fatty liver disease. *World J Gastroenterol* 2012;**18**:727–35
- Jung UJ, Choi MS. Obesity and its metabolic complications: the role of adipokines and the relationship between obesity, inflammation, insulin resistance, dyslipidemia and nonalcoholic fatty liver disease. *Int J Mol Sci* 2014;**15**:6184–223
- Samad F, Ruf W. Inflammation, obesity, and thrombosis. *Blood* 2013;**122**:3415–22
- Choi H, Kim S, Mukhopadhyay P, Cho S, Woo J, Storz G, Ryu SE. Structural basis of the redox switch in the OxyR transcription factor. *Cell* 2001;**105**:103–13
- Tanase DM, Gosav EM, Costea CF, Ciocoiu M, Lacatusu CM, Maranduca MA, Ouatu A, Floria M. The intricate relationship between type 2 diabetes mellitus (T2DM), insulin resistance (IR), and nonalcoholic fatty liver disease (NAFLD). *J Diabetes Res* 2020;**2020**:3920196
- Tilg H, Moschen AR, Roden M. NAFLD and diabetes mellitus. *Nat Rev Gastroenterol Hepatol* 2017;**14**:32–42
- Brunt EM, Wong VW, Nobili V, Day CP, Sookoian S, Maher JJ, Bugianesi E, Sirlin CB, Neuschwander-Tetri BA, Rinella ME. Nonalcoholic fatty liver disease. *Nat Rev Dis Primers* 2015;**1**:15080
- Satapathy SK, Sanyal AJ. Epidemiology and natural history of non-alcoholic fatty liver disease. *Semin Liver Dis* 2015;**35**:221–35
- Friedman SL, Neuschwander-Tetri BA, Rinella M, Sanyal AJ. Mechanisms of NAFLD development and therapeutic strategies. *Nat Med* 2018;**24**:908–22
- Kwong A, Kim WR, Lake JR, Smith JM, Schladt DP, Skeans MA, Noreen SM, Foutz J, Miller E, Snyder JJ, Israni AK, Kasiske BL. OPTN/SRTR 2018 annual data report: liver. *Am J Transplant* 2020;**20**(Suppl s1):193–299
- Goldberg D, Ditah IC, Saeian K, Lalehzari M, Aronsohn A, Gorospe EC, Charlton M. Changes in the prevalence of hepatitis C virus infection, nonalcoholic steatohepatitis, and alcoholic liver disease among patients with cirrhosis or liver failure on the waitlist for liver transplantation. *Gastroenterology* 2017;**152**:1090–9.e1
- Eslam M, Sanyal AJ, George J. International consensus P. MAFLD: a consensus-driven proposed nomenclature for metabolic associated fatty liver disease. *Gastroenterology* 2020;**158**:1999–2014.e1
- Polyzos SA, Kang ES, Boutari C, Rhee EJ, Mantzoros CS. Current and emerging pharmacological options for the treatment of nonalcoholic steatohepatitis. *Metabolism* 2020;**111S**:154203
- Kostrzewski T, Maraver P, Ouro-Gnao L, Levi A, Snow S, Miedzik A, Rombouts K, Hughes D. A microphysiological system for studying nonalcoholic steatohepatitis. *Hepatal Commun* 2020;**4**:77–91

38. Lee-Montiel FT, George SM, Gough AH, Sharma AD, Wu J, DeBiasio R, Vernetti LA, Taylor DL. Control of oxygen tension recapitulates zone-specific functions in human liver microphysiology systems. *Exp Biol Med* 2017;**242**:1617–32
39. Li X, George SM, Vernetti L, Gough AH, Taylor DL. A glass-based, continuously zoned and vascularized human liver acinus microphysiological system (vLAMPs) designed for experimental modeling of diseases and ADME/TOX. *Lab Chip* 2018;**18**:2614–31
40. Feaver RE, Cole BK, Lawson MJ, Hoang SA, Marukian S, Blackman BR, Figureler RA, Sanyal AJ, Wamhoff BR, Dash A. Development of an in vitro human liver system for interrogating nonalcoholic steatohepatitis. *JCI Insight* 2016;**1**:e90954
41. Davidson MD, Kukla DA, Khetani SR. Microengineered cultures containing human hepatic stellate cells and hepatocytes for drug development. *Integr Biol* 2017;**9**:662–77
42. Sahai A, Malladi P, Pan X, Paul R, Melin-Aldana H, Green RM, Whittington PF. Obese and diabetic db/db mice develop marked liver fibrosis in a model of nonalcoholic steatohepatitis: role of short-form leptin receptors and osteopontin. *Am J Physiol Gastrointest Liver Physiol* 2004;**287**:G1035–43
43. Jahn D, Kircher S, Hermanns HM, Geier A. Animal models of NAFLD from a hepatologist's point of view. *Biochim Biophys Acta Mol Basis Dis* 2019;**1865**:943–53
44. Rinella ME, Green RM. The methionine-choline deficient dietary model of steatohepatitis does not exhibit insulin resistance. *J Hepatol* 2004;**40**:47–51
45. Santhekadur PK, Kumar DP, Sanyal AJ. Preclinical models of non-alcoholic fatty liver disease. *J Hepatol* 2018;**68**:230–7
46. Kohli R, Kirby M, Xanthakos SA, Softic S, Feldstein AE, Saxena V, Tang PH, Miles L, Miles MV, Balistreri WF, Woods SC, Seeley RJ. High-fructose, medium chain trans fat diet induces liver fibrosis and elevates plasma coenzyme Q9 in a novel murine model of obesity and nonalcoholic steatohepatitis. *Hepatology* 2010;**52**:934–44
47. Romeo S, Sanyal A, Valenti L. Leveraging human genetics to identify potential new treatments for fatty liver disease. *Cell Metab* 2020;**31**:35–45
48. Eslam M, Valenti L, Romeo S. Genetics and epigenetics of NAFLD and NASH: clinical impact. *J Hepatol* 2018;**68**:268–79
49. Abul-Husn NS, Cheng X, Li AH, Xin Y, Schurmann C, Stevis P, Liu Y, Kozlitina J, Stender S, Wood GC, Stepanchick AN, Still MD, McCarthy S, O'Dushlaine C, Packer JS, Balasubramanian S, Gosalia N, Esopi D, Kim SY, Mukherjee S, Lopez AE, Fuller ED, Penn J, Chu X, Luo JZ, Mirshahi UL, Carey DJ, Still CD, Feldman MD, Small A, Damrauer SM, Rader DJ, Zambrowicz B, Olson W, Murphy AJ, Borecki IB, Shuldiner AR, Reid JG, Overtton JD, Yancopoulos GD, Hobbs HH, Cohen JC, Gottesman O, Teslovich TM, Baras A, Mirshahi T, Gromada J, Dewey FE. A Protein-Truncating HSD17B13 variant and protection from chronic liver disease. *N Engl J Med* 2018;**378**:1096–106
50. Mancina RM, Matikainen N, Maglio C, Söderlund S, Lundbom N, Hakkarainen A, Rametta R, Mozzi E, Fargion S, Valenti L, Romeo S, Taskiran MR, Borén J. Paradoxical dissociation between hepatic fat content and de novo lipogenesis due to PNPLA3 sequence variant. *J Clin Endocrinol Metab* 2015;**100**:E821–5
51. Vernetti LA, Senutovitch N, Boltz R, DeBiasio R, Shun TY, Gough A, Taylor DA. Human liver microphysiology platform for investigating physiology, drug safety, and disease models. *Exp Biol Med* 2016;**241**:101–14
52. Low LA, Mummery C, Berridge BR, Austin CP, Tagle DA. Organs-on-chips: into the next decade. *Nat Rev Drug Discov* 2020;doi: 10.1038/s41573-020-0079-3
53. Mukherjee S, Zhelmin L, Sanfiz A, Pan J, Li Z, Yarde M, McCarty J, Jarai G. Development and validation of an in vitro 3D model of NASH with severe fibrotic phenotype. *Am J Transl Res* 2019;**11**:1531–40
54. Vernetti L, Gough A, Baetz N, Blutt S, Broughman JR, Brown JA, Foulke-Abel J, Hasan N, In J, Kelly E, Kovbasnjuk O, Reppe J, Senutovitch N, Stabb J, Yeung C, Zachos NC, Donowitz M, Estes M, Himmelfarb J, Truskey G, Wikswo JP, Taylor DL. Functional coupling of human microphysiology systems: intestine, liver, kidney proximal tubule, blood-brain barrier and skeletal muscle. *Sci Rep* 2017;**7**:42296
55. Clark AM, Ma B, Taylor DL, Griffith L, Wells A. Liver metastases: microenvironments and ex-vivo models. *Exp Biol Med* 2016;**241**:1639–52
56. Miedel MT, Gavlock DC, Jia S, Gough A, Taylor DL, Stern AM. Modeling the effect of the metastatic microenvironment on phenotypes conferred by estrogen receptor mutations using a human liver microphysiological system. *Sci Rep* 2019;**9**:8341
57. Sakolish C, Reese CE, Luo Y-S, Valdiviezo A, Schurdak ME, Gough A, Taylor DL, Chiu WA, Vernetti LA, Rusyn I. Analysis of reproducibility and robustness of a human microfluidic four-cell liver acinus microphysiology system (LAMPs). *Toxicology* 2021;**448**:152651
58. Sakolish C, Vernetti L, Taylor DL, Rusyn I. Testing of the UPitt Liver Model by the Tex-Val TCTC, https://mps.csb.pitt.edu/assays/assays_tudysset/22/ (2020, accessed 3 April 2021)
59. Novak R, Ingram M, Marquez S, Das D, Delahanty A, Herland A, Maoz BM, Jeanty SSF, Somayaji MR, Burt M, Calamari E, Chalkiadaki A, Cho A, Choe Y, Chou DB, Crouce M, Dauth S, Divic T, Fernandez-Alcon J, Ferrante T, Ferrier J, FitzGerald EA, Fleming R, Jalili-Firoozinezhad S, Grevesse T, Goss JA, Hamkins-Indik T, Henry O, Hinojosa C, Huffstater T, Jang KJ, Kujala V, Leng L, Mannix R, Milton Y, Nawroth J, Nestor BA, Ng CF, O'Connor B, Park TE, Sanchez H, Sliz J, Sontheimer-Phelps A, Swenor B, Thompson G, 2nd, Touloumes GJ, Tranchemontagne Z, Wen N, Yadid M, Bahinski A, Hamilton GA, Levner D, Levy O, Przekwas A, Prantil-Baun R, Parker KK, Ingber DE. Robotic fluidic coupling and interrogation of multiple vascularized organ chips. *Nat Biomed Eng* 2020;**4**:407–20
60. Takeishi K, Collin de l'Hortet A, Wang Y, Handa K, Guzman-Lepe J, Matsubara K, Morita K, Jang S, Haep N, Florentino RM, Yuan F, Fukumitsu K, Tobita K, Sun W, Franks J, Delgado ER, Shapiro EM, Fraunhofer NA, Duncan AW, Yagi H, Mashimo T, Fox IJ, Soto-Gutierrez A. Assembly and function of a bioengineered human liver for transplantation generated solely from induced pluripotent stem cells. *Cell Rep* 2020;**31**:107711
61. Mihaela Z, Srinivasan C, Massoud V, Christina H, Tingting W, Roberto G, Ewa E, Kristina K, Alexandra CdlH, Kazuki T, Alejandro S-G, Strom SC. Guide to the assessment of mature liver gene expression in stem cell-derived hepatocytes. *Stem Cells Develop* 2019;**28**:907–19
62. Jang S, Collin de l'Hortet A, Soto-Gutierrez A. Induced pluripotent stem cell-derived endothelial cells: overview, current advances, applications, and future directions. *Am J Pathol* 2019;**189**:502–12
63. Collin de l'Hortet A, Takeishi K, Guzman-Lepe J, Morita K, Achreja A, Popovic B, Wang Y, Handa K, Mittal A, Meurs N, Zhu Z, Weinberg F, Salomon M, Fox IJ, Deng CX, Nagrath D, Soto-Gutierrez A. Generation of human fatty livers using custom-engineered induced pluripotent stem cells with modifiable SIRT1 metabolism. *Cell Metab* 2019;**30**:385–401.e9
64. Alford FP, Blood SR, Nabarro JD. Glucagon levels in normal and diabetic subjects: use of a specific immunoabsorbent for glucagon radioimmunoassay. *Diabetologia* 1977;**13**:1–6
65. Chitturi S, Abeygunasekera S, Farrell GC, Holmes-Walker J, Hui JM, Fung C, Karim R, Lin R, Samarasinghe D, Liddle C, Weltman M, George J. NASH and insulin resistance: insulin hypersecretion and specific association with the insulin resistance syndrome. *Hepatology* 2002;**35**:373–9
66. Kim NH, Kim DL, Choi KM, Baik SH, Choi DS. Serum insulin, proinsulin and proinsulin/insulin ratio in type 2 diabetic patients: as an index of beta-cell function or insulin resistance. *Korean J Intern Med* 2000;**15**:195–201
67. de Almeida IT, Cortez-Pinto H, Fidalgo G, Rodrigues D, Camilo ME. Plasma total and free fatty acids composition in human non-alcoholic steatohepatitis. *Clin Nutr* 2002;**21**:219–23
68. Tarantino G, Conca P, Riccio A, Tarantino M, Di Minno MN, Chianese D, Pasanisi F, Contaldo F, Scopacasa F, Capone D. Enhanced serum concentrations of transforming growth factor-beta1 in simple fatty liver: is it really benign? *J Transl Med* 2008;**6**:72
69. Harte AL, da Silva NF, Creely SJ, McGee KC, Billyard T, Youssef-Elabd EM, Tripathi G, Ashour E, Abdalla MS, Sharada HM, Amin AI, Burt AD, Kumar S, Day CP, McTernan PG. Elevated endotoxin levels in non-alcoholic fatty liver disease. *J Inflamm* 2010;**7**:15

70. Taylor DL, Wang YL. Fluorescently labeled molecules as probes of the structure and function of living cells. *Nature* 1980;**284**:405–10
71. Giuliano KA, Taylor DL, Waggoner AS. Reagents to measure and manipulate cell functions. *Methods Mol Biol* 2007;**356**:141–63
72. Seward HE, Bagshaw CR. The photochemistry of fluorescent proteins: implications for their biological applications. *Chem Soc Rev* 2009;**38**:2842–51
73. Zhang J, Campbell RE, Ting AY, Tsien RY. Creating new fluorescent probes for cell biology. *Nat Rev Mol Cell Biol* 2002;**3**:906–18
74. Ferrari E, Palma C, Vesentini S, Occhetta P, Rasponi M. Integrating biosensors in organs-on-Chip devices: a perspective on current strategies to monitor microphysiological systems. *Biosensors* 2020;**10**:doi: 10.3390/bios10090110
75. Newman RH, Zhang J. The design and application of genetically encodable biosensors based on fluorescent proteins. *Methods Mol Biol* 2014;**1071**:1–16
76. Lin W, Mehta S, Zhang J. Genetically encoded fluorescent biosensors illuminate kinase signaling in cancer. *J Biol Chem* 2019;**294**:14814–22
77. Belousov VV, Fradkov AF, Lukyanov KA, Staroverov DB, Shakhbazov KS, Terskikh AV, Lukyanov S. Genetically encoded fluorescent indicator for intracellular hydrogen peroxide. *Nat Methods* 2006;**3**:281–6
78. Christian M, Zhang X, Schneider-Merck T, Unterman TG, Gellersen B, White JO, Broens JJ. Cyclic AMP-induced forkhead transcription factor, FKHR, cooperates with CCAAT/enhancer-binding protein beta in differentiating human endometrial stromal cells. *J Biol Chem* 2002;**277**:20825–32
79. Fan W, Morinaga H, Kim JJ, Bae E, Spann NJ, Heinz S, Glass CK, Olefsky JM. FoxO1 regulates Tlr4 inflammatory pathway signalling in macrophages. *EMBO J* 2010;**29**:4223–36
80. Chen Z, Yu R, Xiong Y, Du F, Zhu S. Correction to: a vicious circle between insulin resistance and inflammation in nonalcoholic fatty liver disease. *Lipids Health Dis* 2018;**17**:33
81. Matsuzaki H, Daitoku H, Hatta M, Tanaka K, Fukamizu A. Insulin-induced phosphorylation of FKHR (Foxo1) targets to proteasomal degradation. *Proc Natl Acad Sci U S A* 2003;**100**:11285–90
82. Nakae J, Kitamura T, Silver DL, Accili D. The forkhead transcription factor Foxo1 (fkh) confers insulin sensitivity onto glucose-6-phosphatase expression. *J Clin Invest* 2001;**108**:1359–67
83. Wu Y, Pan Q, Yan H, Zhang K, Guo X, Xu Z, Yang W, Qi Y, Guo CA, Hornsby C, Zhang L, Zhou A, Li L, Chen Y, Zhang W, Sun Y, Zheng H, Wondisford F, He L, Guo S. Novel mechanism of Foxo1 phosphorylation in glucagon signaling in control of glucose homeostasis. *Diabetes* 2018;**67**:2167–82
84. Adachi M, Osawa Y, Uchinami H, Kitamura T, Accili D, Brenner DA. The forkhead transcription factor FoxO1 regulates proliferation and transdifferentiation of hepatic stellate cells. *Gastroenterology* 2007;**132**:1434–46
85. Paschen M, Moede T, Leibiger B, Jacob S, Bryzgalova G, Leibiger IB, Berggren PO. Non-invasive cell type selective in vivo monitoring of insulin resistance dynamics. *Sci Rep* 2016;**6**:21448
86. Kim OK, Jun W, Lee J. Mechanism of ER stress and inflammation for hepatic insulin resistance in obesity. *Ann Nutr Metab* 2015;**67**:218–27
87. Arab JP, Arrese M, Trauner M. Recent insights into the pathogenesis of nonalcoholic fatty liver disease. *Annu Rev Pathol* 2018;**13**:321–50
88. Hashimoto T, Segawa H, Okuno M, Kano H, Hamaguchi HO, Haraguchi T, Hiraoka Y, Hasui S, Yamaguchi T, Hirose F, Osumi T. Active involvement of micro-lipid droplets and lipid-droplet-associated proteins in hormone-stimulated lipolysis in adipocytes. *J Cell Sci* 2012;**125**:6127–36
89. Hsieh K, Lee YK, Londos C, Raaka BM, Dalen KT, Kimmel AR. Perilipin family members preferentially sequester to either triacylglycerol-specific or cholesteryl-ester-specific intracellular lipid storage droplets. *J Cell Sci* 2012;**125**:4067–76
90. Nougarede A, Tesniere C, Ylanko J, Rimokh R, Gillet G, Andrews DW. Improved IRE1 and PERK pathway sensors for multiplex endoplasmic reticulum stress assay reveal stress response to nuclear dyes used for image segmentation. *Assay Drug Dev Technol* 2018;**16**:350–60
91. Zhang XQ, Xu CF, Yu CH, Chen WX, Li YM. Role of endoplasmic reticulum stress in the pathogenesis of nonalcoholic fatty liver disease. *World J Gastroenterol* 2014;**20**:1768–76
92. Malhi H, Kaufman RJ. Endoplasmic reticulum stress in liver disease. *J Hepatol* 2011;**54**:795–809
93. Lebeauin C, Vallee D, Hazari Y, Hetz C, Chevet E, Bailly-Maitre B. Endoplasmic reticulum stress signalling and the pathogenesis of non-alcoholic fatty liver disease. *J Hepatol* 2018;**69**:927–47
94. Iwaisako K, Jiang C, Zhang M, Cong M, Moore-Morris TJ, Park TJ, Liu X, Xu J, Wang P, Paik YH, Meng F, Asagiri M, Murray LA, Hofmann AF, Iida T, Glass CK, Brenner DA, Kisseleva T. Origin of myofibroblasts in the fibrotic liver in mice. *Proc Natl Acad Sci U S A* 2014;**111**:E3297–305
95. Meurer SK, Alsamman M, Sahin H, Wasmuth HE, Kisseleva T, Brenner DA, Trautwein C, Weiskirchen R, Scholten D. Overexpression of endoglin modulates TGF-beta1-signalling pathways in a novel immortalized mouse hepatic stellate cell line. *PLoS One* 2013;**8**:e56116
96. Hung YP, Yellen G. Live-cell imaging of cytosolic NADH-NAD+ redox state using a genetically encoded fluorescent biosensor. *Methods Mol Biol* 2014;**1071**:83–95
97. Goodman RP, Calvo SE, Mootha VK. Spatiotemporal compartmentalization of hepatic NADH and NADPH metabolism. *J Biol Chem* 2018;**293**:7508–16
98. Zhao Y, Shen Y, Wen Y, Campbell RE. High-performance intensimetric direct- and inverse-response genetically encoded biosensors for citrate. *ACS Central Sci* 2020;**8**:1441–1450
99. Iacobazzi V, Infantino V. Citrate—new functions for an old metabolite. *Biol Chem* 2014;**395**:387–99
100. Harada K, Ito M, Wang X, Tanaka M, Wongso D, Konno A, Hirai H, Hirase H, Tsuboi T, Kitaguchi T. Red fluorescent protein-based cAMP indicator applicable to optogenetics and in vivo imaging. *Sci Rep* 2017;**7**:7351
101. Le A, Stine ZE, Nguyen C, Afzal J, Sun P, Hamaker M, Siegel NM, Gouw AM, Kang BH, Yu SH, Cochran RL, Sailor KA, Song H, Dang CV. Tumorigenicity of hypoxic respiring cancer cells revealed by a hypoxia-cell cycle dual reporter. *Proc Natl Acad Sci U S A* 2014;**111**:12486–91
102. Regot S, Hughey JJ, Bajar BT, Carrasco S, Covert MW. High-sensitivity measurements of multiple kinase activities in live single cells. *Cell* 2014;**157**:1724–34
103. Ponugoti B, Dong G, Graves DT. Role of forkhead transcription factors in diabetes-induced oxidative stress. *Exp Diabetes Res* 2012;**2012**:939751
104. Lee S, Dong HH. FoxO integration of insulin signaling with glucose and lipid metabolism. *J Endocrinol* 2017;**233**:R67–R79
105. IOS, Zhang W, Wasserman DH, Liew CW, Liu J, Paik J, DePinho RA, Stolz DB, Kahn CR, Schwartz MW, Unterman TG. FoxO1 integrates direct and indirect effects of insulin on hepatic glucose production and glucose utilization. *Nat Commun* 2015;**6**:7079
106. Fukuda M, Jones JE, Olson D, Hill J, Lee CE, Gautron L, Choi M, Zigman JM, Lowell BB, Elmquist JK. Monitoring FoxO1 localization in chemically identified neurons. *J Neurosci* 2008;**28**:13640–8
107. Lee JW, Chen H, Pullikotil P, Quon MJ. Protein kinase A-alpha directly phosphorylates FoxO1 in vascular endothelial cells to regulate expression of vascular cellular adhesion molecule-1 mRNA. *J Biol Chem* 2011;**286**:6423–32
108. Zhang YS, Aleman J, Shin SR, Kilic T, Kim D, Mousavi Shaegh SA, Massa S, Riahi R, Chae S, Hu N, Avci H, Zhang W, Silvestri A, Sanati Nezhad A, Manbohi A, De Ferrari F, Polini A, Calzone G, Shaikh N, Alerasool P, Budina E, Kang J, Bhise N, Ribas J, Pourmand A, Skardal A, Shupe T, Bishop CE, Dokmeci MR, Atala A, Khademhosseini A. Multisensor-integrated organs-on-chips platform for automated and continual in situ monitoring of organoid behaviors. *Proc Natl Acad Sci U S A* 2017;**114**:E2293–e302
109. Kilic T, Navaee F, Stradolini F, Renaud P, Carrara S. Organs-on-chip monitoring: sensors and other strategies. *Microphysiol Syst* 2018;**2**:doi: 10.21037/mps.2018.01.01

110. Mukherjee A, Repina NA, Schaffer DV, Kane RS. Optogenetic tools for cell biological applications. *J Thorac Dis* 2017;**9**:4867–70
111. Kennedy MJ, Hughes RM, Peteya LA, Schwartz JW, Ehlers MD, Tucker CL. Rapid blue-light-mediated induction of protein interactions in living cells. *Nat Methods* 2010;**7**:973–5
112. Buckley CE, Moore RE, Reade A, Goldberg AR, Weiner OD, Clarke JDW. Reversible optogenetic control of subcellular protein localization in a live vertebrate embryo. *Dev Cell* 2016;**36**:117–26
113. Crefcoeur RP, Yin R, Ulm R, Halazonetis TD. Ultraviolet-B-mediated induction of protein-protein interactions in mammalian cells. *Nat Commun* 2013;**4**:1779
114. Christie JM, Gawthorne J, Young G, Fraser NJ, Roe AJ. LOV to BLUF: flavoprotein contributions to the optogenetic toolkit. *Mol Plant* 2012;**5**:533–44
115. Repina NA, Bao X, Zimmermann JA, Joy DA, Kane RS, Schaffer DV. Optogenetic control of wnt signaling for modeling early embryonic patterning with human pluripotent stem cells. *bioRxiv* 2019;doi: 10.1101/665695
116. Repina NA, McClave T, Johnson HJ, Bao X, Kane RS, Schaffer DV. Engineered illumination devices for optogenetic control of cellular signaling dynamics. *Cell Rep* 2020;**31**:107737
117. Lippincott-Schwartz J, Patterson GH. Photoactivatable fluorescent proteins for diffraction-limited and super-resolution imaging. *Trends Cell Biol* 2009;**19**:555–65
118. Lakhin AV, Tarantul VZ, Gening LV. Aptamers: problems, solutions and prospects. *Acta Naturae* 2013;**5**:34–43
119. Zhou Q, Patel D, Kwa T, Haque A, Matharu Z, Stybayeva G, Gao Y, Diehl AM, Revzin A. Liver injury-on-a-chip: microfluidic co-cultures with integrated biosensors for monitoring liver cell signaling during injury. *Lab Chip* 2015;**15**:4467–78
120. Choi J-H, Lee J, Shin W, Choi J-W, Kim HJ. Priming nanoparticle-guided diagnostics and therapeutics towards human organs-on-chips microphysiological system. *Nano Converg* 2016;**3**:24
121. Bhowmick T, Berk E, Cui X, Muzykantov VR, Muro S. Effect of flow on endothelial endocytosis of nanocarriers targeted to ICAM-1. *J Control Release* 2012;**157**:485–92
122. Wang XD, Stolwijk JA, Lang T, Sperber M, Meier RJ, Wegener J, Wolfbeis OS. Ultra-small, highly stable, and sensitive dual nanosensors for imaging intracellular oxygen and pH in cytosol. *J Am Chem Soc* 2012;**134**:17011–4
123. Chandra A, Prasad S, Gigli G, del Mercato LL. Chapter 6 – fluorescent nanoparticles for sensing. In: WJ Parak, N Feliu (eds) *Frontiers of nanoscience*. Amsterdam: Elsevier, 2020, pp. 117–49
124. Subiros-Funosas R, Mendive-Tapia L, Sot J, Pound JD, Barth N, Varela Y, Goni FM, Paterson M, Gregory CD, Albericio F, Dransfield I, Lavilla R, Vendrell M. A Trp-BODIPY cyclic peptide for fluorescence labelling of apoptotic bodies. *Chem Commun* 2017;**53**:945–8
125. Barth ND, Subiros-Funosas R, Mendive-Tapia L, Duffin R, Shields MA, Cartwright JA, Henriques ST, Sot J, Goni FM, Lavilla R, Marwick JA, Vermeren S, Rossi AG, Egeblad M, Dransfield I, Vendrell MA. Fluorogenic cyclic peptide for imaging and quantification of drug-induced apoptosis. *Nat Commun* 2020;**11**:4027
126. Mendive-Tapia L, Wang J, Vendrell M. Fluorescent cyclic peptides for cell imaging. *Peptide Sci* 2020;**e24181**. doi: 10.1002/pep2.24181
127. Fam TK, Klymchenko AS, Collet M. Recent advances in fluorescent probes for lipid droplets. *Materials* 2018;**11**:1768
128. Zheng Y, Miyamoto DT, Wittner BS, Sullivan JP, Aceto N, Jordan NV, Yu M, Karabacak NM, Comaills V, Morris R, Desai R, Desai N, Emmons E, Milner JD, Lee RJ, Wu CL, Sequist LV, Haas W, Ting DT, Toner M, Ramaswamy S, Maheswaran S, Haber DA. Expression of beta-globin by cancer cells promotes cell survival during blood-borne dissemination. *Nat Commun* 2017;**8**:14344
129. Peng Y, Wen D, Lin F, Mahato RI. Co-delivery of siAlox15 and sunitinib for reversing the new-onset of type 1 diabetes in non-obese diabetic mice. *J Control Rel* 2018;**292**:1–12
130. Donato MT, Tolosa L. Stem-cell derived hepatocyte-like cells for the assessment of drug-induced liver injury. *Differentiation* 2019;**106**:15–22
131. Rezvani M, Grimm AA, Willenbring H. Assessing the therapeutic potential of lab-made hepatocytes. *Hepatology* 2016;**64**:287–94
132. Liu JT, Lamprecht MP, Duncan SA. Using human induced pluripotent stem cell-derived hepatocyte-like cells for drug discovery. *J Vis Exp* 2018;**135**:57194
133. Dao Thi VL, Wu X, Belote RL, Andreo U, Takacs CN, Fernandez JP, Vale-Silva LA, Prallet S, Decker CC, Fu RM, Qu B, Uryu K, Molina H, Saeed M, Steinmann E, Urban S, Singaraja RR, Schneider WM, Simon SM, Rice CM. Stem cell-derived polarized hepatocytes. *Nat Commun* 2020;**11**:1677
134. Baudy AR, Otieno MA, Hewitt P, Gan J, Roth A, Keller D, Sura R, Van Vleet TR, Proctor WR. Liver microphysiological systems development guidelines for safety risk assessment in the pharmaceutical industry. *Lab on a Chip* 2019;**20**:215–25
135. Du Y, Khandekar G, Llewellyn J, Polacheck W, Chen CS, Wells RG. A bile duct-on-a-chip with organ-level functions. *Hepatology* 2019;**71**:1350–63
136. de Raemy-Schenk AM, Trouble S, Gaillard P, Page P, Gotteland JP, Scheer A, Lang P, Yeow K. A cellular assay for measuring the modulation of glucose production in H4IIE cells. *Assay Drug Dev Technol* 2006;**4**:525–33
137. Porter WH, Yao HH, Karounos DG. Laboratory and clinical evaluation of assays for beta-hydroxybutyrate. *Am J Clin Pathol* 1997;**107**:353–8
138. Giobbe GG, Michielin F, Luni C, Giulitti S, Martewicz S, Dupont S, Floreani A, Elvassore N. Functional differentiation of human pluripotent stem cells on a chip. *Nat Methods* 2015;**12**:637–40
139. Mosoyan G, Kraus T, Ye F, Eng K, Crispino J, Hoffman R, Iancu-Rubin C. Imetelstat, a telomerase inhibitor, differentially affects normal and malignant megakaryopoiesis. *Leukemia* 2017;**31**:2458
140. Reinicke M, Becker S, Ceglarek U. LC-MS/MS analysis of triglycerides in blood-derived samples. *Methods Mol Biol* 2018;**1730**:111–21
141. Puri P, Daita K, Joyce A, Mirshahi F, Santhekadur PK, Cazanave S, Luketic VA, Siddiqui MS, Boyett S, Min HK, Kumar DP, Kohli R, Zhou H, Hylemon PB, Contos MJ, Idowu M, Sanyal AJ. The presence and severity of nonalcoholic steatohepatitis is associated with specific changes in circulating bile acids. *Hepatology* 2018;**67**:534–48
142. Wang R, Ding Q, Yaqoob U, de Assuncao TM, Verma VK, Hirsova P, Cao S, Mukhopadhyay D, Huebert RC, Shah VH. Exosome adherence and internalization by hepatic stellate cells triggers sphingosine 1-phosphate-dependent migration. *J Biol Chem* 2015;**290**:30684–96
143. Cao Y, Kamioka Y, Yokoi N, Kobayashi T, Hino O, Onodera M, Mochizuki N, Nakae J. Interaction of FoxO1 and TSC2 induces insulin resistance through activation of the mammalian target of rapamycin/p70 S6K pathway. *J Biol Chem* 2006;**281**:40242–51
144. Harlen K, Quinn J, Hughes T, Quinn AM. New fluorescent tools to monitor cell stress and toxicity. SLAS 2018 Poster, 2018
145. Wilhelmsen K, Farrar K, Hellman J. Quantitative in vitro assay to measure neutrophil adhesion to activated primary human microvascular endothelial cells under static conditions. *J Vis Exp* 2013;**78**:e50677
146. Barros LF, Bittner CX, Loaiza A, Ruminot I, Larenas V, Moldenhauer H, Oyarzun C, Alvarez M. Kinetic validation of 6-NBDG as a probe for the glucose transporter GLUT1 in astrocytes. *J Neurochem* 2009;**109**(Suppl 1):94–100
147. Caldwell S, Ikura Y, Dias D, Isomoto K, Yabu A, Moskaluk C, Pramoonjago P, Simmons W, Scruggs H, Rosenbaum N, Wilkinson T, Toms P, Argo CK, Al-Osaimi AM, Redick JA. Hepatocellular ballooning in NASH. *J Hepatol* 2010;**53**:719–23
148. Benedicto A, Romayor I, Arteta B. Role of liver ICAM-1 in metastasis. *Oncol Lett* 2017;**14**:3883–92
149. Stark R, Grzelak M, Hadfield J. RNA sequencing: the teenage years. *Nat Rev Genet* 2019;**20**:631–56
150. Hoang SA, Oseini A, Feaver RE, Cole BK, Asgharpour A, Vincent R, Siddiqui M, Lawson MJ, Day NC, Taylor JM, Wamhoff BR, Mirshahi F, Contos MJ, Idowu M, Sanyal AJ. Gene expression predicts histological severity and reveals distinct molecular profiles of nonalcoholic fatty liver disease. *Sci Rep* 2019;**9**:12541
151. Pedersen HD, Galsgaard ED, Christoffersen B, Cirera S, Holst D, Fredholm M, Latta M. NASH-inducing diets in Göttingen minipigs. *J Clin Exp Hepatol* 2020;**10**:211–21
152. Church RJ, Kullak-Ublick GA, Aubrecht J, Bonkovsky HL, Chalasani N, Fontana RJ, Goepfert JC, Hackman F, King NMP, Kirby S, Kirby P,

- Marcinak J, Ormarsdottir S, Schomaker SJ, Schuppe-Koistinen I, Wolenski F, Arber N, Merz M, Sauer JM, Andrade RJ, van Bömmel F, Poynard T, Watkins PB. Candidate biomarkers for the diagnosis and prognosis of drug-induced liver injury: an international collaborative effort. *Hepatology* 2019;**69**:760–73
153. Norona LM, Nguyen DG, Gerber DA, Presnell SC, Mosedale M, Watkins PB. Bioprinted liver provides early insight into the role of Kupffer cells in TGF-beta1 and methotrexate-induced fibrogenesis. *PLoS One* 2019;**14**:e0208958
154. Norona LM, Nguyen DG, Gerber DA, Presnell SC, LeCluyse EL. Editor's highlight: modeling compound-induced fibrogenesis in vitro using three-dimensional bioprinted human liver tissues. *Toxicol Sci* 2016;**154**:354–67
155. Bulutoglu B, Rey-Bedon C, Kang YBA, Mert S, Yarmush ML, Usta OB. A microfluidic patterned model of non-alcoholic fatty liver disease: applications to disease progression and zonation. *Lab Chip* 2019;**19**:3022–31
156. Jang KJ, Otieno MA, Ronxhi J, Lim HK, Ewart L, Kodella KR, Petropolis DB, Kulkarni G, Rubins JE, Conegliano D, Nawroth J, Simic D, Lam W, Singer M, Barale E, Singh B, Sonee M, Streeter AJ, Manthey C, Jones B, Srivastava A, Andersson LC, Williams D, Park H, Barrile R, Sliz J, Herland A, Haney S, Karalis K, Ingber DE, Hamilton GA. Reproducing human and cross-species drug toxicities using a liver-chip. *Sci Transl Med* 2019;**11**:eaax5516
157. Lee DW, Lee SH, Choi N, Sung JH. Construction of pancreas-muscle-liver microphysiological system (MPS) for reproducing glucose metabolism. *Biotechnol Bioeng* 2019;**116**:3433–45
158. Tan K, Keegan P, Rogers M, Lu M, Gosset JR, Charest J, Bale SS. A high-throughput microfluidic microphysiological system (PREDICT-96) to recapitulate hepatocyte function in dynamic, re-circulating flow conditions. *Lab Chip* 2019;**19**:1556–66
159. Nawroth J, Petropolis DB, Manatakis D, Maulana T, Burchett G, Schlunder K, Witt A, Shukla A, Hamilton GA, Ekihiro S, Lu S, Karalis K. Modeling alcoholic liver disease in a human liver-chip. *bioRxiv* 2020;doi: 10.1101/2020.07.14.203166
160. Younossi ZM, Golabi P, de Avila L, Paik JM, Srishord M, Fukui N, Qiu Y, Burns L, Afendy A, Nader F. The global epidemiology of NAFLD and NASH in patients with type 2 diabetes: a systematic review and meta-analysis. *J Hepatol* 2019;**71**:793–801
161. Grundy SM, Hansen B, Smith SC, Jr., Cleeman JI, Kahn RA, American Heart A, National Heart L, Blood I, American DA. Clinical management of metabolic syndrome: report of the American Heart Association/National Heart, Lung, and Blood Institute/American Diabetes Association Conference on scientific issues related to management. *Circulation* 2004;**109**:551–6
162. Hasnain M, Vieweg WV, Fredrickson SK, Beatty-Brooks M, Fernandez A, Pandurangi AK. Clinical monitoring and management of the metabolic syndrome in patients receiving atypical antipsychotic medications. *Prim Care Diab* 2009;**3**:5–15
163. Huang G, Coviello A. Clinical update on screening, diagnosis and management of metabolic disorders and cardiovascular risk factors associated with polycystic ovary syndrome. *Curr Opin Endocrinol Diab Obesity* 2012;**19**:512–9
164. Farrell GC, Haczeyni F, Chitturi S. Pathogenesis of NASH: how metabolic complications of overnutrition favour lipotoxicity and pro-inflammatory fatty liver disease. *Adv Exp Med Biol* 2018;**1061**:19–44
165. De Chiara F, Heeboll S, Marrone G, Montoliu C, Hamilton-Dutoit S, Ferrandez A, Andreola F, Rombouts K, Gronbaek H, Felipe V, Gracia-Sancho J, Mookerjee RP, Vilstrup H, Jalan R, Thomsen KL. Urea cycle dysregulation in non-alcoholic fatty liver disease. *J Hepatol* 2018;**69**:905–15
166. Eriksen PL, Vilstrup H, Rigbolt K, Suppli MP, Sorensen M, Heeboll S, Veidal SS, Knop FK, Thomsen KL. Non-alcoholic fatty liver disease alters expression of genes governing hepatic nitrogen conversion. *Liver Int* 2019;**39**:2094–101
167. Lieber CS. Relationships between nutrition, alcohol use, and liver disease. *Alcohol Res Health* 2003;**27**:220–31
168. Thomsen KL, Gronbaek H, Glavind E, Hebbard L, Jessen N, Clouston A, George J, Vilstrup H. Experimental nonalcoholic steatohepatitis compromises ureagenesis, an essential hepatic metabolic function. *Am J Physiol Gastrointest Liver Physiol* 2014;**307**:G295–301
169. Hadizadeh F, Faghihmani E, Adibi P. Nonalcoholic fatty liver disease: diagnostic biomarkers. *World J Gastrointest Pathophysiol* 2017;**8**:11–26
170. Miyazaki M, Kato M, Tanaka K, Tanaka M, Kohjima M, Nakamura K, Enjoji M, Nakamuta M, Kotoh K, Takayanagi R. Increased hepatic expression of dipeptidyl peptidase-4 in non-alcoholic fatty liver disease and its association with insulin resistance and glucose metabolism. *Mol Med Rep* 2012;**5**:729–33
171. Wang L, Yu S, Chan A. Pathology of non-alcoholic fatty liver disease. *Int J Dig Dis* 2016;**2**:1–7
172. Tsuchida T, Friedman SL. Mechanisms of hepatic stellate cell activation. *Nat Rev Gastroenterol Hepatol* 2017;**14**:397–411
173. Arriazu E, Ruiz de Galarreta M, Cubero FJ, Varela-Rey M, Perez de Obanos MP, Leung TM, Lopategi A, Benedicto A, Abraham-Enachescu I, Nieto N. Extracellular matrix and liver disease. *Antioxid Redox Signal* 2014;**21**:1078–97
174. Dewidar B, Meyer C, Dooley S, Meindl-Beinker AN. TGF-beta in hepatic stellate cell activation and liver fibrogenesis-updated 2019. *Cells* 2019;**8**:1419
175. Okazaki I, Noro T, Tsutsui N, Yamanouchi E, Kuroda H, Nakano M, Yokomori H, Inagaki Y. Fibrogenesis and carcinogenesis in nonalcoholic steatohepatitis (NASH): involvement of matrix metalloproteinases (MMPs) and tissue inhibitors of metalloproteinase (TIMPs). *Cancers* 2014;**6**:1220–55
176. Turner M, Chantry D, Feldmann M. Transforming growth factor beta induces the production of interleukin 6 by human peripheral blood mononuclear cells. *Cytokine* 1990;**2**:211–6
177. Schmidt-Arras D, Rose-John S. IL-6 pathway in the liver: from physiopathology to therapy. *J Hepatol* 2016;**64**:1403–15
178. Panesar N, Tolman K, Mazuski JE. Endotoxin stimulates hepatocyte interleukin-6 production. *J Surg Res* 1999;**85**:251–8
179. Koyama Y, Brenner DA. Liver inflammation and fibrosis. *J Clin Invest* 2017;**127**:55–64
180. Katsarou A, Moustakas II, Pyrina I, Lembessis P, Koutsilieris M, Chatzigeorgiou A. Metabolic inflammation as an instigator of fibrosis during non-alcoholic fatty liver disease. *World J Gastroenterol* 2020;**26**:1993–2011
181. Enzan H, Toi M, Hayashi Y, Hamauzu T, Kuroda N, Hiroi M. *Zone 3 predominance of histopathological features in nonalcoholic steatohepatitis. NASH and nutritional therapy*. Springer: Verlag Tokyo, 2005, pp.50–7
182. Chalasani N, Wilson L, Kleiner DE, Cummings OW, Brunt EM, Unalp A, Network NCR. Relationship of steatosis grade and zonal location to histological features of steatohepatitis in adult patients with non-alcoholic fatty liver disease. *J Hepatol* 2008;**48**:829–34
183. Niederreiter L, Tilg H. Cytokines and fatty liver diseases. *Liver Res* 2018;**2**:14–20
184. Shi J, Fan J, Su Q, Yang Z. Cytokines and abnormal glucose and lipid metabolism. *Front Endocrinol* 2019;**10**:703
185. Tilg H, Moschen AR. Insulin resistance, inflammation, and non-alcoholic fatty liver disease. *Trends Endocrinol Metab* 2008;**19**:371–9
186. Tan Z, Liu Q, Jiang R, Lv L, Shoto SS, Maillat I, Quesniaux V, Tang J, Zhang W, Sun B, Ryffel B. Interleukin-33 drives hepatic fibrosis through activation of hepatic stellate cells. *Cell Mol Immunol* 2018;**15**:388–98
187. Jiao J, Ooka K, Fey H, Fiel M, Rahhman A, Kojima K, Hoshida Y, Chen X, de Paula T, Vetter D, Sastre D, Lee KH, Lee YA, Bansal M, Friedman S, Merad M, Aloman C. Interleukin-15 receptor α on hepatic stellate cells regulates hepatic fibrogenesis in mice. *J Hepatol* 2016;**65**:344–53
188. Zhou Z, Xu MJ, Cai Y, Wang W, Jiang JX, Varga ZV, Feng D, Pacher P, Kunos G, Torok NJ, Gao B. Neutrophil-hepatic stellate cell interactions promote fibrosis in experimental steatohepatitis. *Cell Mol Gastroenterol Hepatol* 2018;**5**:399–413
189. Mamontova AV, Solov'yev ID, Savitsky AP, Shakhov AM, Lukyanov KA, Bogdanov AM. Bright GFP with subnanosecond fluorescence lifetime. *Sci Rep* 2018;**8**:13224
190. Merzlyak EM, Goedhart J, Shcherbo D, Bulina ME, Shcheglov AS, Fradkov AF, Gaintzeva A, Lukyanov KA, Lukyanov S, Gadella TWJ,

- Chudakov DM. Bright monomeric red fluorescent protein with an extended fluorescence lifetime. *Nat Methods* 2007;**4**:555–7
191. Natarajan V, Berglund EJ, Chen DX, Kidambi S. Substrate stiffness regulates primary hepatocyte functions. *RSC Adv* 2015;**5**:80956–66
192. Xia T, Zhao R, Feng F, Yang L. The effect of matrix stiffness on human hepatocyte migration and function – an in vitro research. *Polymers* 2020;**12**:1903
193. Sano E, Mori C, Matsuoka N, Ozaki Y, Yagi K, Wada A, Tashima K, Yamasaki S, Tanabe K, Yano K, Torisawa Y-S. Tetrafluoroethylene-propylene elastomer for fabrication of microfluidic organs-on-chips resistant to drug absorption. *Micromachines* 2019;**10**:793
194. Domansky K, Sliz JD, Wen N, Hinojosa C, Thompson G, Fraser JP, Hamkins-Indik T, Hamilton GA, Levner D, Ingber DE. SEBS elastomers for fabrication of microfluidic devices with reduced drug absorption by injection molding and extrusion. *Microfluid Nanofluid* 2017;**21**:107
195. Wikswo JP, Curtis EL, Eagleton ZE, Evans BC, Kole A, Hofmeister LH, Matloff WJ. Scaling and systems biology for integrating multiple organs-on-a-chip. *Lab Chip* 2013;**13**:3496–511
196. Prill S, Bavli D, Levy G, Ezra E, Schmalzlin E, Jaeger MS, Schwarz M, Duschl C, Cohen M, Nahmias Y. Real-time monitoring of oxygen uptake in hepatic bioreactor shows CYP450-independent mitochondrial toxicity of acetaminophen and amiodarone. *Arch Toxicol* 2016;**90**:1181–91
197. Bavli D, Prill S, Ezra E, Levy G, Cohen M, Vinken M, Vanfleteren J, Jaeger M, Nahmias Y. Real-time monitoring of metabolic function in liver-on-chip microdevices tracks the dynamics of mitochondrial dysfunction. *Proc Natl Acad Sci U S A* 2016;**113**:E2231–40
198. Ehrlich A, Tsytkin-Kirschenschweig S, Ioannidis K, Ayyash M, Riu A, Note R, Ouedraogo G, Vanfleteren J, Cohen M, Nahmias Y. Microphysiological flux balance platform unravels the dynamics of drug induced steatosis. *Lab Chip* 2018;**18**:2510–22
199. Wikswo JP, Block FE, III, Cliffler DE, Goodwin CR, Marasco CC, Markov DA, McLean DL, McLean JA, McKenzie JR, Reiserer RS, Samson PC, Schaffer DK, Seale KT, Sherrod SD. Engineering challenges for instrumenting and controlling integrated organ-on-chip systems. *IEEE Transac Biomed Eng* 2013;**60**:682–90